Pergamon

Journal of Structural Geology, Vol. 17, No. 7, pp. 927 to 948, 1995

0191-8141/95 $9.50+0.00

0191-8141(94)00113-8

Strain ellipsoids from incompetent dykes: application to volume loss during mylonitization in the Singö gneiss zone, central Sweden

CHRISTOPHER J. TALBOT and DIMITRIOS SOKOUTIS

Hans Ramberg Tectonic Laboratory, Institute of Earth Sciences, Uppsala University, Norbyvägen 18B, S-751-36 Uppsala, Sweden

(*Received* 13 *December* 1991; *accepted in revised form* 29 *September* 1994)

Cheshire-Cat: "You see, a dog growls when it's angry, and wags it's tail when it's pleased. Now *I* growl when I'm pleased, and wag my tail when I'm angry."

The Cheshire-Cat vanished quite slowly, beginning with the end of the tail, and ending with the grin, which remained some time after the rest of it had gone.

(Carroll 1865)

Abstract—We describe how to constrain bulk strain ellipsoids by distinguishing the attitudes of mullioned from planar contacts in incompetent dykes. Our method is demonstrated by using metabasaltic dykes to construct strain ellipsoids ($X \geq Y \geq Z$) in the Palaeoproterozoic Singö deformation zone of Sweden. Ductile flows are found empirically to be homogeneous within two scale-ranges: 2–10 m localities in a 3 × 3 km district. These alternate with three scale-ranges in which inhomogeneous strains generated decimetre-scale mullions and 30 m wide mylonites in a gneiss zone over 3 km wide. X axes in locality ellipsoids rotate from subhorizontal in Singö gneisses with natural strains of $\bar{\varepsilon}_s \approx 1.2$, to subvertical in mylonites ($2 < \bar{\varepsilon}_s < 3$) and ultramylonites ($\bar{\varepsilon}_s > 3$) where X parallels the ubiquitous mineral lineation.

Several of the theoretical limitations of working with homogeneous strains can be bypassed in practice. Tie-lines between ellipsoids constructed by applying different methods to different markers in the same rocks demonstrate that our *strain field* is also the *strain path*. Individual ellipsoids are constructed assuming no volume change—but their strain path reveals a uniaxial volume loss of ≈3% per 10% total shortening of Z in an otherwise pure shear. Replotting locality ellipsoids with respect to the orientation of the district ellipsoid reveals that gneisses in the Singö zone are the result of cryptic (≈1.86–1.83 Ga) transpression that led to (≈1.83–1.6 Ga) extrusion along dip-flow mylonites of gneiss lenses that may be the roots of former nappes.

INTRODUCTION

Like other peneplained collages of continental Precambrian crust, the crystalline basement of Fennoscandia consists of terranes constructed in different environments being sutured together along zones of intense deformation. Many such deformation zones have been identified because swarms of mafic sheets are deformed within them and not in adjacent terranes (Båk *et al.* 1975, Gorbatschev & Bogdanova 1993). Mafic inclusions, so obvious among granitoid rocks, are particularly useful strain markers where they have deformed as competent single layers. However, the structures that develop in incompetent mafic sheets deformed at higher temperature are much less well understood (Passchier *et al.* 1990).

We all recognize the buckles and boudins that develop in deformed competent single layers—but what happens when incompetent mafic sheets deform faster than their granitoid country rocks? They develop a strong internal foliation and structures called mullions (Wilson 1961, Ramsay 1967).

Mullions are cylindrical deformation structures in a single interface that in axial profile display sharp cusps alternating with rounded lobes (Fletcher 1982). Wilson (1961) distinguished four types of mullions but most recent studies have been on those in strain-active contacts shortened along their length (Smith 1975, 1977, Sokoutis 1987, 1990). There is general agreement that mullion cusps point away from incompetent layers. However, there is confusion over how mullions in shortened contacts can be distinguished from those in elongated contacts and whether they interfere across single layers to folds or inverse folds (Talbot & Sokoutis 1992). Part of this confusion is because mullions develop in single contacts but pinches and folds require mullions on two surfaces to interfere across a single intervening layer.

We have found that the internal foliation distinguishes mullions along shortened and elongated contacts (Talbot & Sokoutis 1992). The foliation is axial planar to mullions in shortened contacts and at angles >45° to those contacts (Fig. 1). By contrast, the foliation nearly parallels the elongated contacts of inverse folds (Fig. 1).

The only documented examples of inverse folds that we know of are our own (Talbot & Sokoutis 1992). Indeed, only a few other workers have even mentioned that mullions occur in the contacts of incompetent layers (e.g. Ramsay 1967). Instead, most have concentrated on the foliation. Foliations that are strong in mafic inclusions and weaker or even absent from their country rock have been attributed to magma globules having

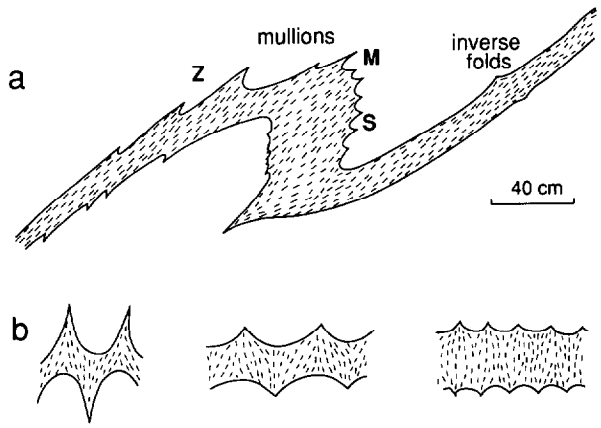

Fig. 1. (a) Cartoon of a deformed incompetent mafic dyke indicating its sigmoidal and zigmoidal internal foliation and s, z and m-shaped mullions along its shortened contacts and an inverse fold along an elongated limb. (b) The decrease in ratio of mullion wavelength to layer thickness indicates decreasing competence contrast between shortened incompetent layers and their hosts (Sokoutis 1987, 1990). In the Singö zone, ratios of mullion wavelength to dyke thickness are generally so small that mullions are typically disharmonic across dykes 0.1–1 m thick. The sketch on the far right is therefore more typical of the Singö region than the class-3 fold shown on the far left.

been deformed to schlieren (Vernon 1984) or to meta-igneous sheets that were either still molten (Kaitero 1953, Watterson 1968, Berger 1971, Pitcher & Berger 1972, Davidson & Park 1978, Smith 1979) or too hot to foliate (Johnson & Dalziel 1966, Allaart 1967) having undergone 'private orogenies' in country rocks that ranged from rigid to molten. All these possibilities are special cases of a more general explanation. Foliated and mullioned inclusions with outward-pointing cusps merely display the symptoms of having deformed faster than their surroundings at any stage during or after their emplacement (Talbot 1982).

Past studies of the foliation within incompetent inclusions have constrained the orientation and symmetry of bulk strains—but not the strain intensities (Talbot 1983). We will argue here that mullions in incompetent dykes are more useful strain markers than their internal foliation. We consider that incompetent strain markers will eventually have as much potential for unravelling strains in the lower crust as competent single layers have had for unravelling strain histories in the upper crust. However, mullions and inverse folds will have to replace buckles and pinches as indicators of progressive strains, and remullioned mullions will have to replace refolded folds as indicators of separable episodes of deformation (Talbot & Sokoutis 1992). Our main aim here is to demonstrate that deformation structures in incompetent single layers allow the empirical determination of domains of homogeneous strains and the measurement of the orientations and shapes of the ellipsoids that describe those strains.

The theory of homogeneous strain has a long pedigree (Becker 1893, Flinn 1962, 1978, Ramsay 1967, 1976, Talbot 1970, 1987, Smith 1975, 1977) and is still under development (Passchier 1990a,b, Weijermars 1993). We start by using this theory to explain how structures due to inhomogeneous strains of incompetent dykes on small scales allow the construction of ellipsoids that describe homogeneous strains on larger scales.

Do deformation zones involve simple biaxial shear? What intensities of strains mylonitize granitoid protoliths? We answer these simple but fundamental questions by applying our new method to a particular example: the Singö zone in central Sweden. The regional setting of the Singö zone and our strain markers are described. Homogeneous strains on scales of localities (2–10 m) and the district (3 × 3 km) are used to comment on the inhomogeneous strains on intervening scales, those responsible for a gneiss zone $>\approx 3$ km wide and mylonites within it that are ≈ 30 m wide. Strains measured by the new method are checked against strains measured using more conventional techniques. Removing the deformation recorded by a dyke swarm from the strains of older enclaves in its country rocks discloses that the Singö zone began with right-handed strike shear in gneisses and then changed to the vertical extrusion of lenses of these gneiss along dip-shear mylonite zones. We end by wondering if the Singö zone was once the root zone to a pile of nappes since lost to erosion.

DEFORMATION OF SINGLE LAYER SUBFABRICS

Imagine a penetrative and homogeneous bulk strain of a rock complex containing single layers with a wide range of orientations (Fig. 2a). The most useful strain markers are veins, sheets or dykes with ratios of length-to-thickness that exceed about 7:1 so that they rotate at the bulk strain rate (Gay 1968). We will show that systematic studies of the structures developed in the contacts of strain-active single layers can recover the ellipsoid that describes the homogeneous bulk strains in each of the blocks shown in Fig. 2.

Strain-passive dykes (Fig. 2c) deform at the same rate as their host rock; no deformation structures develop and the foliation crosses contacts without refraction. Initially spherical passive inclusions distort to strain ellipsoids with shapes and orientations representative of the bulk strain (Fig. 2c). By contrast, initially spherical strain-active inclusions will track the bulk strain path more slowly if they are competent (Fig. 2b) and precede the bulk strain if they are incompetent (Fig. 2d).

Strain-active dykes rotate (change angle) at the same rate as their host—but distort (change length) at different rates (Figs. 2b & d). To change length at the same rate as parallel layers of their host, strain-active layers thicken or thin inhomogeneously by developing cuspate structures. The bulk strain can remain homogeneous because refraction of the foliation across strain-active interfaces (Treagus & Sokoutis 1992) demonstrates that strain inhomogeneities extend no more than a wavelength away from cuspate contacts (Talbot 1982). Similar cusps amplifying along their contacts interfere across single layers less than a wavelength thick to one of four categories of shear instabilities: buckles, pinches, mullions or inverse folds (Smith 1975, 1977).

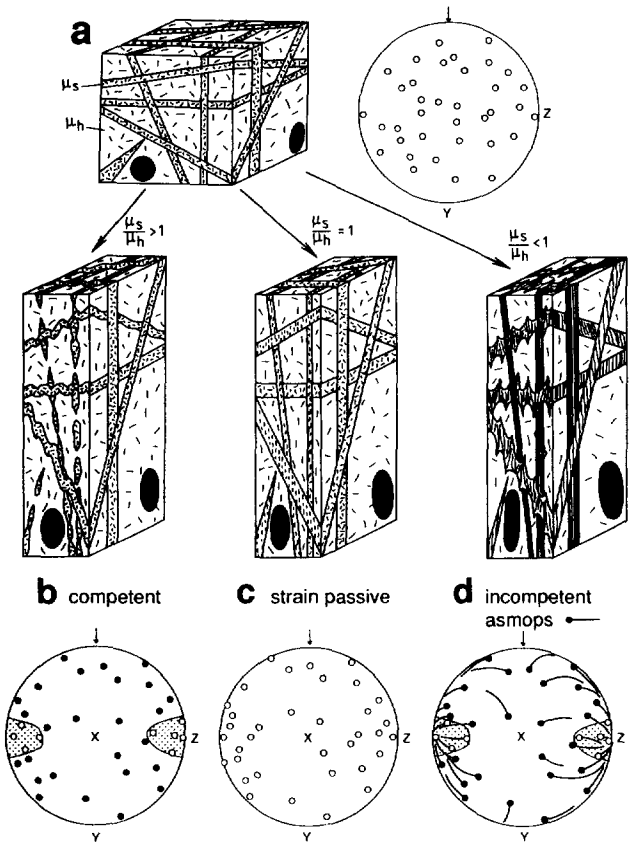

Fig. 2. Homogeneous triaxial flattening of initially spherical inclusions (black) and single layers with length/thickness ratios sufficiently large (>7:1) that they rotate at the bulk strain rate. Initial sheets (in a) change length and thickness more slowly (b), at the same rate (c), and faster (d) than their host depending on how their effective viscosities compare to that of their host. μ_s is the strain rate of the sheets, μ_h the strain rate of the host. Equal-area nets indicate how poles to planar sheet elements fall into an elliptical March concentration centred on *Z* and elongate to *Y*. An elliptical *polar snoe* (shaded) contains poles to planar elements elongated beyond their initial lengths in all directions (open circles) that have thinned uniformly with or without rare pinches (in b) or even more rare inverse folds (in d). Poles to shortened sheet contacts folded (in b) or mullioned (in d) fall outside the *polar snoe* which is centred on *Z* and elongate to *X*. *X* is 90° away from *Z* in the *XZ* plane with *Y* as its pole. *Asmops* (*a*pparent *s*tructural *mo*vement *p*aths) in (d) can be reconstructed by plotting poles to foliation refracted across incompetent layers.

Competent dykes distort more slowly than their surroundings. Uniform thickening or thinning alone does not allow them to shorten or elongate as fast as parallel layers in their host. They keep pace by changing length and thickness by additional and faster mechanisms: they buckle to shorten as fast, or pinch to elongate as rapidly. Many competent layers with orientations that elongate (some after unfolding, see point 1.3 in Appendix) are likely to be sufficiently thin to undergo stable elongation. In that case, rather than amplifying to pinches that might separate to boudins, initial perturbations along their contacts open so that thin layers elongate and thin uniformly (point 2.3 in Appendix). We avoid the term pinch-and-swell because no swelling is involved in layer elongation.

Foliations are generally so much stronger within *incompetent dykes* than in their country rocks that their host rocks are often judged to be free of contemporaneous strain. The foliation is oblique across most incompetent dykes and its intensity commonly diminishes inward from shear zones along the inner sides of their contacts and may disappear entirely in the centres of thick examples (Talbot 1982). The foliation in such marginal shear zones is either sigmoidal or zigmoidal depending on the sense of antithetic internal shear or vorticity they have undergone in response to synthetic bulk shear or spin (Talbot 1982). Incompetent dykes tend to shorten and thicken faster than their surroundings as they rotate at the bulk strain rate. They still thicken uniformly, but the non-uniform layer thickening represented by mullions slows shortening to the bulk strain rate.

Mullions are not likely to amplify in single layer as fast as buckles, and inverse folds are likely to amplify even more slowly (Smith 1977). This explains the relative rarity of mullions and the even greater rarity of inverse folds compared to the buckles and pinches in mafic dykes deformed at lower temperatures. In the district we analyze here, we recognized only a few inverse folds along hundreds of incompetent dykes; most had presumably undergone stable extension and thinned uniformly. The few dykes that developed inverse folds did so to slow their elongation to the bulk strain rate (see point 2.2 in Appendix).

Smith's mathematics (1975, 1977) suggest that mullions should interfere across shortening incompetent layers to symmetric and opposed 'inverse boudins' but experiments (Sokoutis 1987, 1990) and field observations (Talbot 1982, 1983) find that mullions on opposed contacts of the same incompetent layer interfere to form Ramsay's (1967) class-3 folds with the foliation axial planar (Fig. 1a). Similarly, Smith (1975) expected the cusps that point outward from elongated incompetent single layers to interfere to inverse folds—but those we have seen look more like inverse pinches (Fig. 1b) The cusps in the contacts of incompetent dykes are still useful even before we understand this disparity between theory and observation (Talbot & Sokoutis 1992).

Summarizing the deformation of single layers, cusps in folds, pinches, mullions and inverse folds all point towards what was the more competent material across formerly strain-active contacts of planar elements (Fig. 3). All four structures represent different combinations of cusp interference across single layers that shortened-and-thickened or elongated-and-thinned because they had different orientations in a bulk strain. The bulk strain ellipsoid can be constrained by distinguishing the orientation of elongated and shortened planar elements of cusped contacts.

STRAIN ELLIPSOIDS FROM INCOMPETENT SINGLE LAYERS

Surface and polar surface of no elongation (***snoe and polar snoe***)

Shortened and elongated linear or planar markers lie on different sides of the special family of mathematical

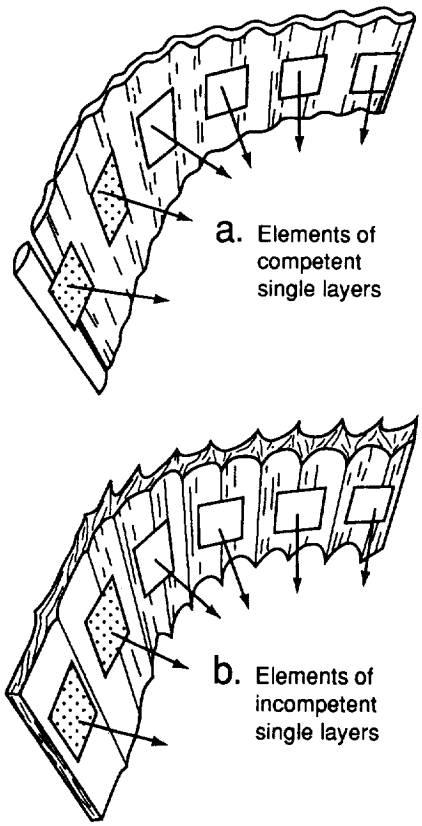

Fig. 3. Planar elements of deformed single layers that are smaller or larger (shaded) than their initial area.

lines that trace the surface of *no* elongation (*snoe*) of that strain. The *snoe* (introduced as the surface of no infinitesimal or finite longitudinal strain by Flinn in 1962) is the double conical surface that joins the line of intersection between a strain ellipsoid and its initial sphere with their common centre (Fig. 4). Flinn (1962) showed how the shape of the *snoe* relates directly to the shape of the strain ellipsoid independent of any volume change.

The shape of the ellipsoid could come from the angular dimensions of the *snoe* itself (as in Flinn 1962). However, we prefer to use a similar immaterial surface, the *polar snoe* traced by *poles* to the *snoe* (Fig. 4). Mapping the *polar snoe* rather than *snoe* sounds like an unnecessary complication but is in fact far more efficient (see Section 2 of Appendix). This is because planar strain markers are generally more common than linear markers in deformed rocks. It is therefore usually easier and more informative to measure the dip and strike of planar markers that have changed in area than it is to measure lines which have changed in length. It may be counter-intuitive, but where linear markers must be artificially created using the intersection of planar markers with the outcrop face, it is easier to directly construct three-dimensional strain ellipsoids than it is to reconstruct two-dimensional strain ellipses.

We therefore follow Talbot (e.g. 1970, 1987) and strip a dimension from the problem by measuring the orientation, symmetry and intensity of strain directly from the orientation, shape and size of the *polar snoe* (see point 2.1 in Appendix). This is done by plotting the perpendiculars to planar elements of deformed dyke contacts (Fig. 3) as *poles* on a lower hemisphere equal-area net (Sellés-Martinez 1993). A boundary is then drawn on the equal-area net to exclude as many as possible poles to shortened (mullioned or folded) elements and include all poles to extended elements (planar, pinched or inversely folded: points 2.2 and 2.3 of Appendix).

The *polar snoe* bounds the field of overall elongation, the field containing poles to planar elements elongated in all directions on an equal-area net (Talbot 1970). Like the *snoe*, the *polar snoe* is symmetrical about the principal axes ($X \geq Y \geq Z$) and planes of the finite strain ellipsoid. However, whereas the *snoe* encloses a central XY plane or X, the longest principal axis of strain, the inverse *polar snoe* is centred on Z, the shortest principal axis of strain.

The graph on Fig. 4 is a convenient visualization of Flinn's (1962) expressions relating the apical angles $\Phi°$ subtended by the boundaries of the *snoe* in two of the three principal planes (and, as labelled on Fig. 4 here, the *polar snoe*). Two of the three values of $\Psi_{ZX}°$, $\Psi_{ZY}°$ or $\Psi_{YX}°$ are sufficient to calculate the axial ratios of strain ellipsoids with constant volumes (Fig. 4). The *snoe* and *polar snoe* are both independent of volume change and the apparent limitation of assuming constant volume (discussed by Ramsay 1976) only applies to each locality. We will show later how integrating ellipsoids from associated localities can bypass this limitation.

Field procedure

Outcrops suitable for mapping the *polar snoe* have strain active markers with both shortened and elongated contacts exposed in appropriate relief. Many markers may have a wide range of orientations (like the competent veins in Jackson & Robertson 1983). The dip and strike of planar elements of incompetent dykes (Fig. 3) are measured distinguishing whether their contacts are planar, inversely folded, or mullioned with s, z or m symmetries. Primary apophyses (Figs. 6e & f) must not be confused with secondary mullions (Fig. 6g)

Shapes and sizes of polar snoe

The location of the *polar snoe* on the equal-area net reflects the orientation of bulk strain, its shape reflects the symmetry of bulk strain, and its size is a measure of bulk strain intensity. For uniaxial oblate ellipsoids, the *polar snoe* is circular and shrinks on a central Z during uniaxial flattening. For triaxial oblate ellipsoids, the *polar snoe* is elliptical and longest in ZX and narrowest in ZY (so that $\Psi_{ZX}° > \Psi_{ZY}°$) and shrinks on its central Z during triaxial flattening. X is 90° away from Z in the XZ plane with Y as its pole (Fig. 4). For biaxial shears the *polar snoe* is merely a line (part of the XZ plane) which shortens towards Z as the shear intensities. Such linear *polar snoes* lie across the widest, central part of the girdle of poles to a planar March fabric (Owens 1974).

There is no field of overall elongation for prolate ellipsoids due to constriction; instead there is an

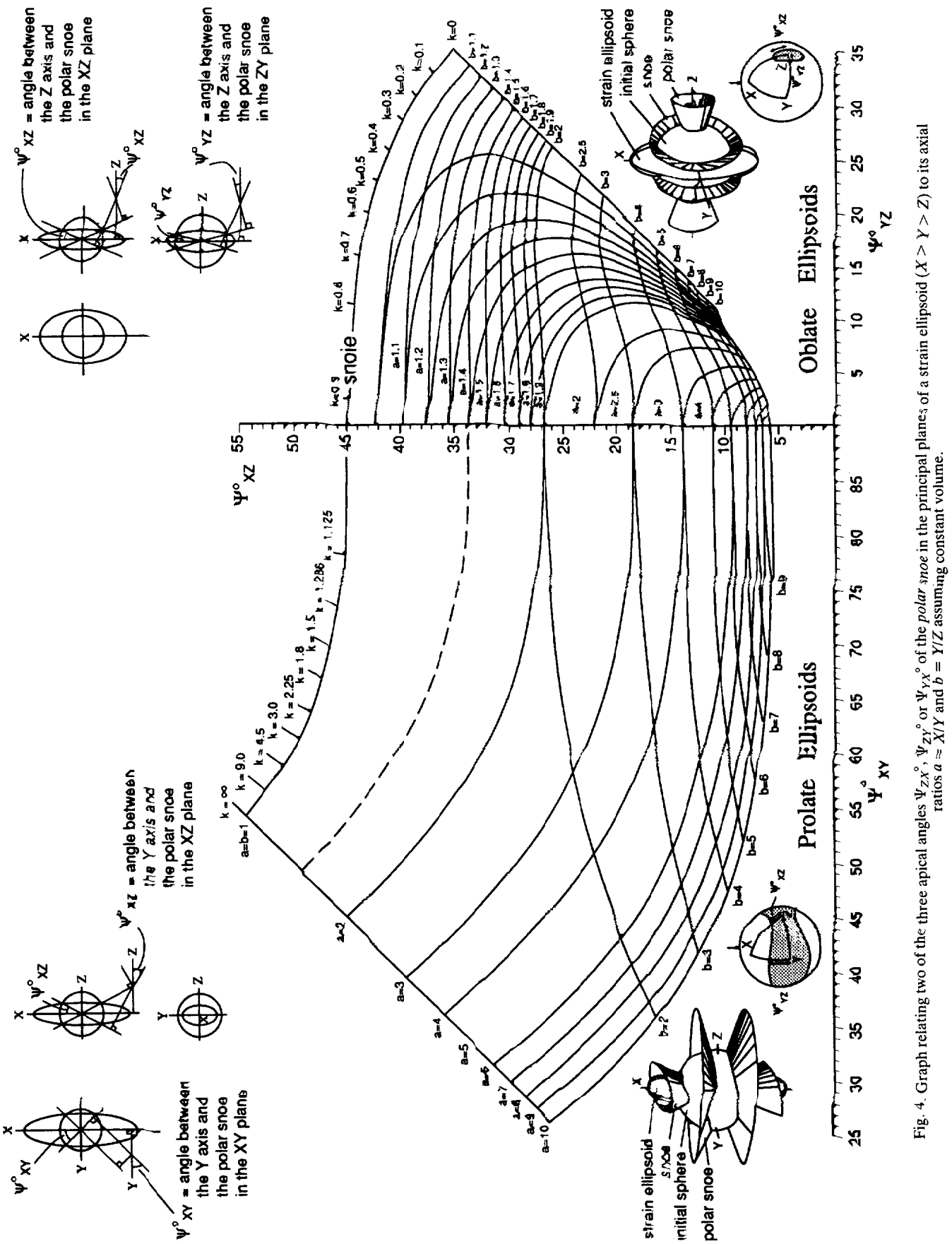

Fig. 4. Graph relating two of the three apical angles Ψ_{ZX}°, Ψ_{ZY}° or Ψ_{YX}° of the *polar snoe* in the principal planes of a strain ellipsoid ($X > Y > Z$) to its axial ratios $a \approx X/Y$ and $b = Y/Z$ assuming constant volume.

equivalent field of overall shortening (Talbot 1970). This field contains all poles to dyke elements that display irregular fold interference patterns because they have shortened in all directions at the same time (see 2.2 in Appendix). The field of overall shortening is circular for uniaxial prolate ellipsoids and elliptical for triaxial, apparently prolate ellipsoids. It obeys all the rules that apply to the field of overall extension, the only difference being that the adjective 'prolate' substitutes for 'oblate'.

In practice (Talbot *et al.* 1987), it is still worth distinguishing the *polar snoe* for constricted rocks. For apparently prolate ellipsoids the *polar snoe* separates an elliptical field of overall shortening from a girdle of elongation. This girdle is narrowest in ZY and widest in the XY plane which is 90° away and has Z as its pole so that $\Psi_{YX}^{\circ} > \Psi_{ZY}^{\circ}$. For uniaxial prolate strains the *polar snoe* is an XY girdle of constant width perpendicular to Z so that $\Psi_{YX}^{\circ} = \Psi_{ZY}^{\circ}$. All the ellipsoids described here from the Singö zone lie in the field of apparent oblate strains. It is therefore inevitable that our application over-emphasizes such cases.

Theoretically, the *polar snoe* for a homogeneous strain is a simple smooth ellipse or girdle (Fig. 4). *Polar snoes* with such simple shapes suggest that the strains of the localities can be considered homogeneous on the scale of data collection. If, by contrast, the boundary of the *polar snoe* is irregular, then *either* the data are insufficient, *or* the bulk strain of the sampled rock mass was inhomogeneous. Including or excluding data from larger or smaller volumes of the same rock complex usually allows empirical recognition of domains for which the strain can be considered homogeneous. In the Singö zone, the country rock foliation is generally planar and of uniform intensity throughout localities which yield simple and useable elliptical *polar snoes*; we rejected pear- or mushroom-shaped *polar snoes* from outcrops with foliations of variable intensity as having come from strain gradients too steep to be considered homogeneous on scales of metres (see point 1.5, Appendix).

The Appendix outlines some of the practical details of mapping *polar snoes*. There we explain that, because mullions unmullion as readily as folds unfold, *polar snoes* with data patterns with symmetries less than orthorombic are among the most obvious symptoms of a locality having undergone bulk rotation (and spun). We also explain why we have been unable to distinguish localities that have spun using the structural complications suggested by Passchier (1990a, b). We illustrate there that rocks do not read textbooks by emphasizing some of the differences between theory and practice. Thus the most and least common structures in deformed single layers anticipated on theoretical grounds differ from those actually found in rocks.

Strain markers other than incompetent dykes

Two more conventional methods were used at some of the same localities to check the strains measured using *polar snoes* of incompetent dykes at 25 localities: (1) the axial ratios of enclaves and their general orientation could be measured at five localities, and (2) the *polar snoe* of competent veins within some of the mafic sheets could be mapped at two localities.

We also mapped in three dimensions what Flinn (1962) called structural movement paths of the foliation within the dykes. Tie-lines between poles to segments of foliation with different orientations on an equal-area net are taken as *a*pparent *s*tructural *mo*vement *p*aths (*asmops*). *Asmops* are interpreted as recording the effects of shear of the same foliation at different rates for the same time (Talbot 1982, 1983, Munier & Talbot 1993). *Asmops* define arcs symmetrical about the principal planes of bulk strain and converge on Z by rotating away from X (Fig. 2d). They approach Y closest in a plane depending on the shape (k or v) of the ellipsoid.

In the early stages of our study of the Singö zone we mapped both *asmops* and *polar snoes* for the same dykes in many of the same localities (Talbot & Sokoutis 1988). However, *asmops* constrain only the orientation and anisotropy of strain and not its intensity. We therefore dropped the tedious observations necessary to recover *asmops* when it became clear that they give only part of the information derived more easily by distinguishing the orientations of mullioned from planar sheet contacts.

THE SINGÖ ZONE AND ITS STRAIN MARKERS

The 2.0–1.8 Ga Svecofennian sialic crust of Sweden appears to have accreted rapidly southwards from an Archaean nucleus in the north (Gaal & Gorbatschev 1987, Gorbatschev & Bogdanova 1993). Steady-state lateral accretion by arc-welding of cold sedimentary prisms was punctuated locally by the suturing of terranes constructed elsewhere (Talbot & Heeroma 1989). Sedimentary prisms survive relatively undisturbed where the magmatic arc behind the subduction zone was extinguished by ocean closure.

East central Sweden (Fig. 5) is characterized by a polygonal network of late Palaeoproterozoic supracrustal belts that surround intrusive granitoid plutons yielding Rb/Sr ages of ≈1.89–1.88 Ga (Welin *et al.* 1980). Most of these supracrustal rocks consist of shelf carbonates interlayered with lavas of rhyolite to dacite, together with agglomerates, tuffs and cherts which merge with siliciclastic sediments.

While the region was still at amphibolite facies, the polygonal map pattern of supracrustal belts was smeared clockwise into the Singö zone (Fig. 5). This zone of gneisses with subvertical WNW-striking foliation is at least 5 km wide onshore and follows the coast near the town of Östhammar (Fig. 5). The gneissose fabric intensifies to mylonitic fabric in three steep zones which are about 30 m wide and trend WNW–ESE across the tiny peninsula at Hamnholm (Fig. 9). Similar mylonites with the same orientation are known alongshore to the west-northwest and southeast and in the Finnish islands of Åland offshore to the east (Ehlers *et al.* 1993).

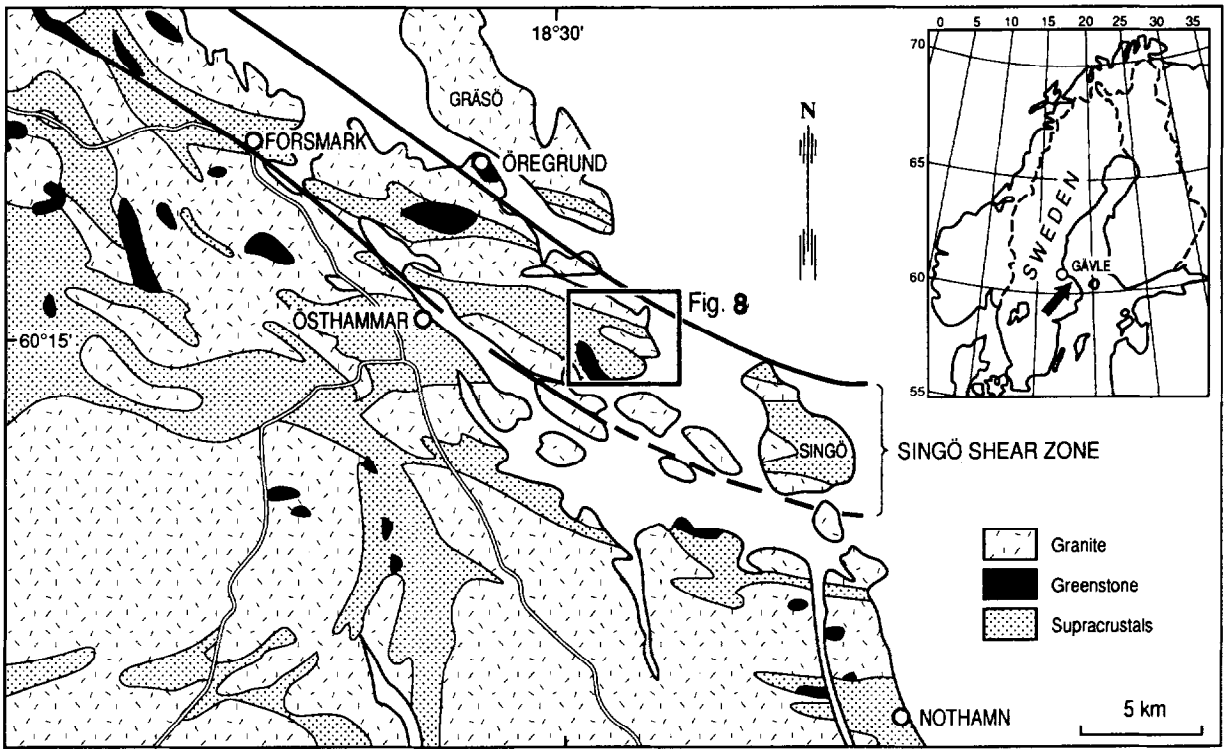

Fig. 5. Simplified geological map of the regions around Östhammar, Sweden. Minimal boundaries to the Singö shear zone have been added and the district studied here is outlined.

The mylonites on Hamnholmen peninsula (Fig. 9) contain centimetre thick seams of cataclasites in ultramylonites and millimetre thick seams of devitrified palaeoseismic fault melts as well as younger faults and fractures. Mineral orientation lineations are generally subvertical while most younger slickenlines are subhorizontal. Although there has been no previous demonstration that the deformation actually involved biaxial shear rather than, say, triaxial transpression, all these symptoms of repeated reactivations of intense shear in different environments have earlier been grouped together under the term Singö shear zone (Carlsson & Christiansson 1986).

Where geophysical maps exist (Henkel 1991) the gneisses, mylonites, faults and fracture zones of the Singö shear zone can be interpolated as anastomosing linear anomalies with general WNW-trends between the island of Singö in the east to at least the town of Gävle in the west (Fig. 5). Geomorphology suggests that the Singö zone may be as much as 50 km wide with most of its width offshore (Eriksson & Henkel 1988). How far this zone extends inland to the northwest of Gävle is not yet clear but the Singö zone may be a strand of a major terrane boundary which extrapolates northwest across Proterozoic Sweden and beneath the Caledonides (Sjöström & Bergman 1993).

The general and engineering geology of the Singö shear zone (Fig. 5) has been documented in various reports (e.g. Carlsson & Christiansson 1986) concerned with excavating Sweden's repository for low and intermediate radioactive wastes near the nuclear power complex at Forsmark (Fig. 5).

The absolute timing of events in the Svecofennian crust near Östhammar are poorly constrained (see review by Tirén 1991). The metasediments and volcanites are probably ≈2.0–1.9 Ga (Lundqvist 1979, Stålhös 1991). Large scale magmatic flow in the plutons appears to have persisted until 1.83 Ga when it accounted for a regional annealing indicated by Rb/Sr cooling ages (Welin *et al.* 1980). The first ductile shear probably began to localize in the Singö gneiss zone while a swarm of mafic (Östhammar) dykes was being emplaced at ≈1.859 Ga (from a U/Pb date on a deformed pegmatite, Welin and Stålhös 1986). The dykes were mylonitized before they were veined by epidote at 300–200°C between 1.6 and 1.5 Ga.

We consider here only the ductile strains in a 3 × 3 km district near Östhammar (Figs. 8 and 9, located on Fig. 5). Being on the coast, this district has the disadvantage that the geology can be seen on only one side of the Singö zone; this disadvantage is compensated by the excellent exposure. Another advantage is that the Singö zone along the coast was probably seismically imaged at middle crustal levels by the BABEL working group (1993). The strains we report here in the Singö mylonites have been used to calibrate *in situ* and laboratory measurements of velocities of seismic and ultrasonic P and S waves with the aim of backward and forward modelling seismic images of the Singö zone (Law 1994). In effect, because of their mafic components and their combined widths, the Singö mylonites can be seismically imaged offsetting the Moho which is ≈46 km deep southwest of the zone and ≈48 km to the northeast (BABEL 1993). Geological reconnaissance associated

with BABEL suggests that the comparitively simple story we develop here is complicated by additional elements elsewhere (Law 1994). Thus mylonites are veined by undeformed (Rapakivi?) granite and offset along north–south shears in adjoining areas.

Strain markers

We chose to study the Singö zone in the district outlined on Fig. 5 because the mafic enclaves and dykes that we used as incompetent strain markers are well exposed there. Indeed, Sederholm introduced the concept of mixing and mingling of mantle and crustal magmas by first documenting and interpreting the backveining of mafic igneous sheets by aplite veins on Åland, an archipelago about 100 km east of Östhammar (Sederholm 1932, see e.g. Mehnert 1968). Enclaves (Figs. 6a–d) represent older mature stages of the Sederholm effect and dykes (Figs. 6e–g and 7a–i) the later and less advanced stages.

Enclaves

Sederholm (1932) explained how simple metabasaltic dykes traced along their length can be increasingly disrupted by veins of aplite obviously derived by melting of country rocks that are usually granitoid plutonic rocks (as in Fig. 6) but can be silicic volcanics (e.g. near Nothamn, Fig. 5). Traced along the mafic dyke, the aplite veins increase in number, width and grain size until they disperse the former dyke to collections of mafic enclaves (Fig. 6). Such enclaves initiated with angular shapes but became rounded as they were dispersed and digested in melts that started granitic but, with continued additions of basalt, hybridized through granodorites to tonalites (Stålhös 1991).

The ambiguity in age of mafic sheets that intrude the granite on a large scale, but are themselves backveined by granitoid melts on smaller scales, is still a constant source of confusion. The granitic melts that backveined and broke up mafic dykes to enclaves and hybridites were melted by the heat advected from the mantle by the basaltic dykes themselves. Mafic sheets displaying the Sederholm effect are like the Cheshire-Cat (Carroll 1865); the enclaves represent the grin that remains after the cat has disappeared; the mafic dykes fade away leaving only the more persistent enclaves as evidence of the body that brought them.

The Sederholm effect is nowadays referred to as magma mixing and mingling; although the terms have changed and the details have been refined (e.g. Vernon 1984, Huppert & Sparks 1988) the original concept remains (Sederholm 1932). In modern terms, basalts among the silicic volcanics (Fig. 6) were pumped from the mantle along dykes through granitoid plutons that were still sufficiently molten to feed the rhyolites. We now know that the viscosity of basalt can be so low (e.g. $\approx$10 Pa s) that it is capable of fracturing paths through granite that is sufficiently stiff to fracture even while it is still molten (10^4–10^{14} Pa s, Cruden 1990). As the mafic sheets froze (at $\approx$1100°C), they shrank about 2 vol% and so were backveined by still (or newly) molten fractions of their silicic surroundings. Until they cooled to $\approx$750°C, the silicic rocks remained molten and the whole complex continued to flow slowly and penetratively. Differential flow dispersed and digested enclaves fragmented from a succession of meta-basaltic sheets in increasingly hybridized plutons (Figs. 6a–e).

Östhammar dyke swarm

Whereas early basaltic dykes intruded into molten and hot granites were dispersed to isolated enclaves (Fig. 6), later dykes survived as the Östhammar dyke swarm (Fig. 7). This swarm is several tens of kilometres wide on land, and trends WNW parallel to the coast through Östhammar (Holst 1887, Stålhos 1991). Where least deformed, the swarm consists of two conjugate sets of anastomosing mafic dykes (Fig. 7a) that trend generally west-northwest and north. Individual dykes commonly display primary bayonet-shaped apophyses (Figs. 6e–g) indicating that they propagated by breaking bridges between short sections with various degrees of en échelon offset and overlap (Nicholson & Pollard 1985). The acute angle between these two sets of dilated shears opens northwest–southeast from a subvertical axis of intersection (Fig. 7a). We therefore follow Roberts (1970) and infer that mantle basalts dilated anastomosing paths sheared through silicic crust at significant depth. The stress field induced by mantle melts during brief episodes of magma cracking had a horizontal northwest–southeast maximum compression axis and a vertical axis of intermediate stress (similar to current *in situ* stresses which are in the wrench regime below a surficial thrust regime $\approx$400 m thick, Tirén 1991). Magma pressures therefore appear to have temporarily inverted the long term stress field likely to be responsible from the subvertical WNW-foliation in the Singö gneiss zone. The last of the Östhammer dykes were therefore probably being emplaced while the strains we describe in the next section were first beginning to generate the Singö gneiss zone (at $\approx$1.86 Ga).

RESULTS

Shears within the Singö gneiss and mylonite zone

Locality ellipsoids ($>2\ m < 10\ m$). Our primary strain data are fully documented in Figs. 8 and 9. The structures along the contacts of *incompetent* dykes at 25 localities (and *competent* quartzofeldspathic veins within the mafic dykes at two of them) are shown on lower hemisphere equal-area nets together with the *polar snoes* and principal axes ($X \geq Y \geq Z$) and planes of the strain ellipsoids interpreted from them. Listed around each equal-area net are: (1) $\Psi_{YZ}{}^\circ$ and $\Psi_{XZ}{}^\circ$, the angular dimensions of the *polar snoe* in the principal planes; (2) the axial ratios $a = X/Y$ and $b = Y/Z$, assuming no volume change; (3) the direction

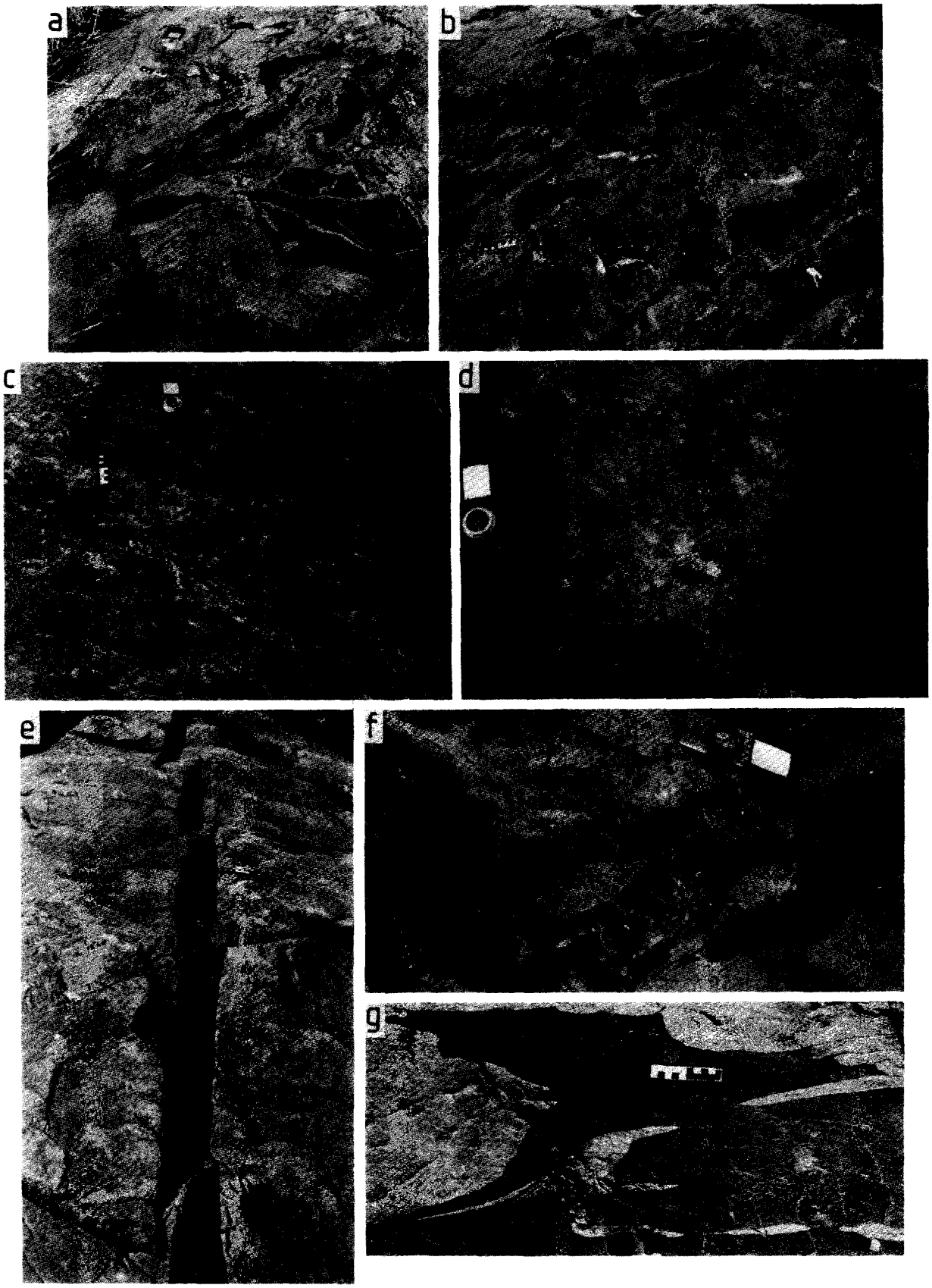

Fig. 6. (a) & (b) The Sederholm effect on the island of Gräsö (Fig. 5). Mafic sheets back-veined by silicic melts are dispersed as enclaves with Cheshire-Cat-like grins in hybridized granitoids. (c) Enclaves about 40 m, and (d) 20 m away from mylonites, northernmost Hamnholmen (Fig. 9). (e) Primary bridges and apophyses along a weakly deformed Östhammar dyke. (f) Deformed bridges and apophyses. (g) Aplite veins folded and boudinaged inside a mullioned mafic sheet ≈100 m northwest of locality 24.

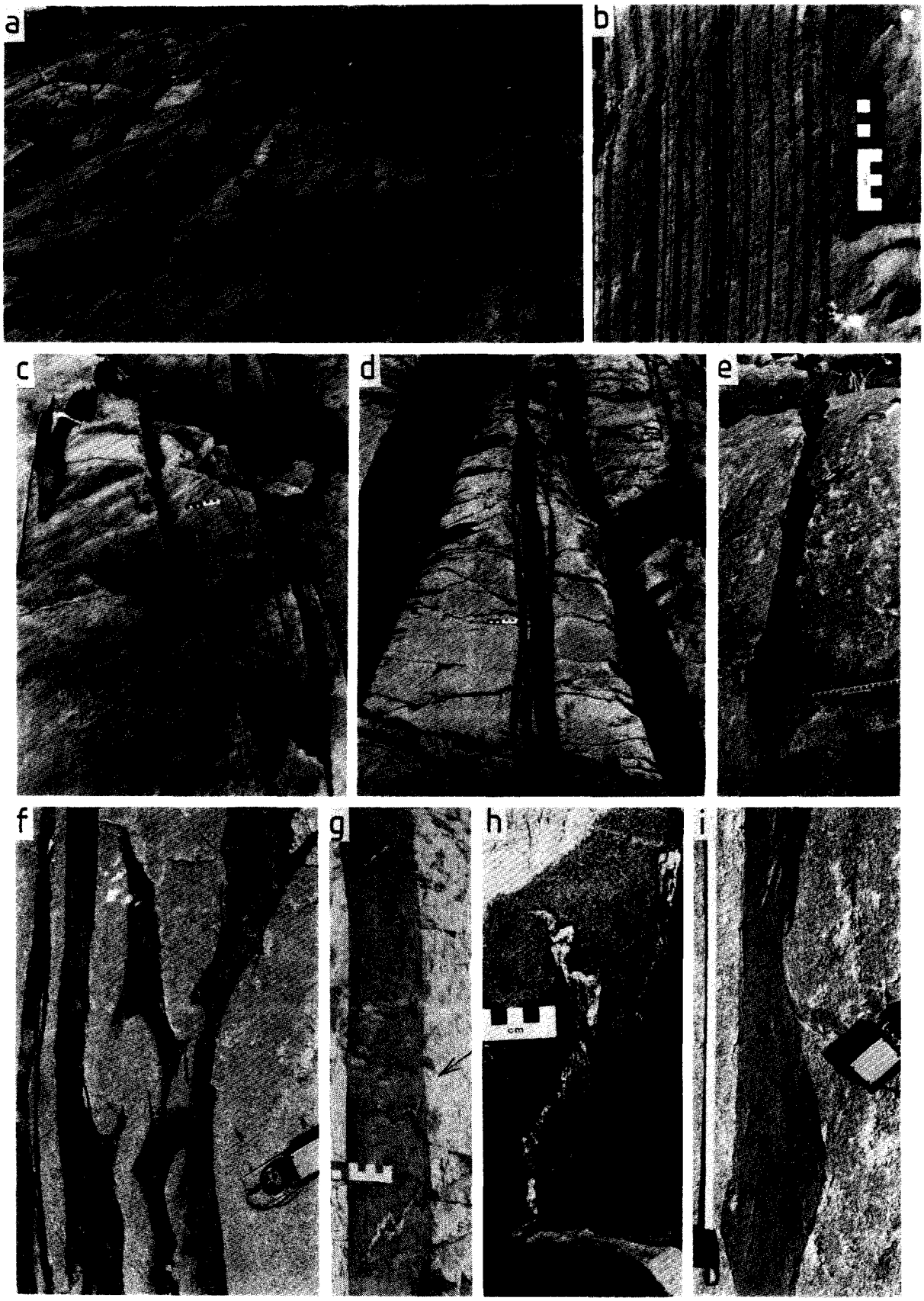

Fig. 7. (a) General view of decimetre to metre-wide dykes of Östhammar dyke swarm ($\bar{\varepsilon}_3 \approx 1.2$) looking east-southeast from locality 22. (b) Dykes in the most intense mylonite ($\bar{\varepsilon}_3 > 3$) near locality 20, Hamnholm peninsula, contrast with protolith in (a). (c) Shortened dykes are mullioned. (d) Screens of country rock are pinched inside elongated but planar mafic dykes. (e) Inverse folds along elongated dyke near locality 4. (f) Screens of country rock pinched and folded inside mafic dykes. (g) Quartzo-feldspathic veins folded ($\bar{\varepsilon}_3 \approx 1.7$) inside mafic dyke at locality 15 ($\bar{\varepsilon}_3 \approx 2.9$). (h) Subvertical fold hinges and mineral lineation in quartzo-feldspathic vein at locality 14. (i) Close up of inverse folds in (e) above.

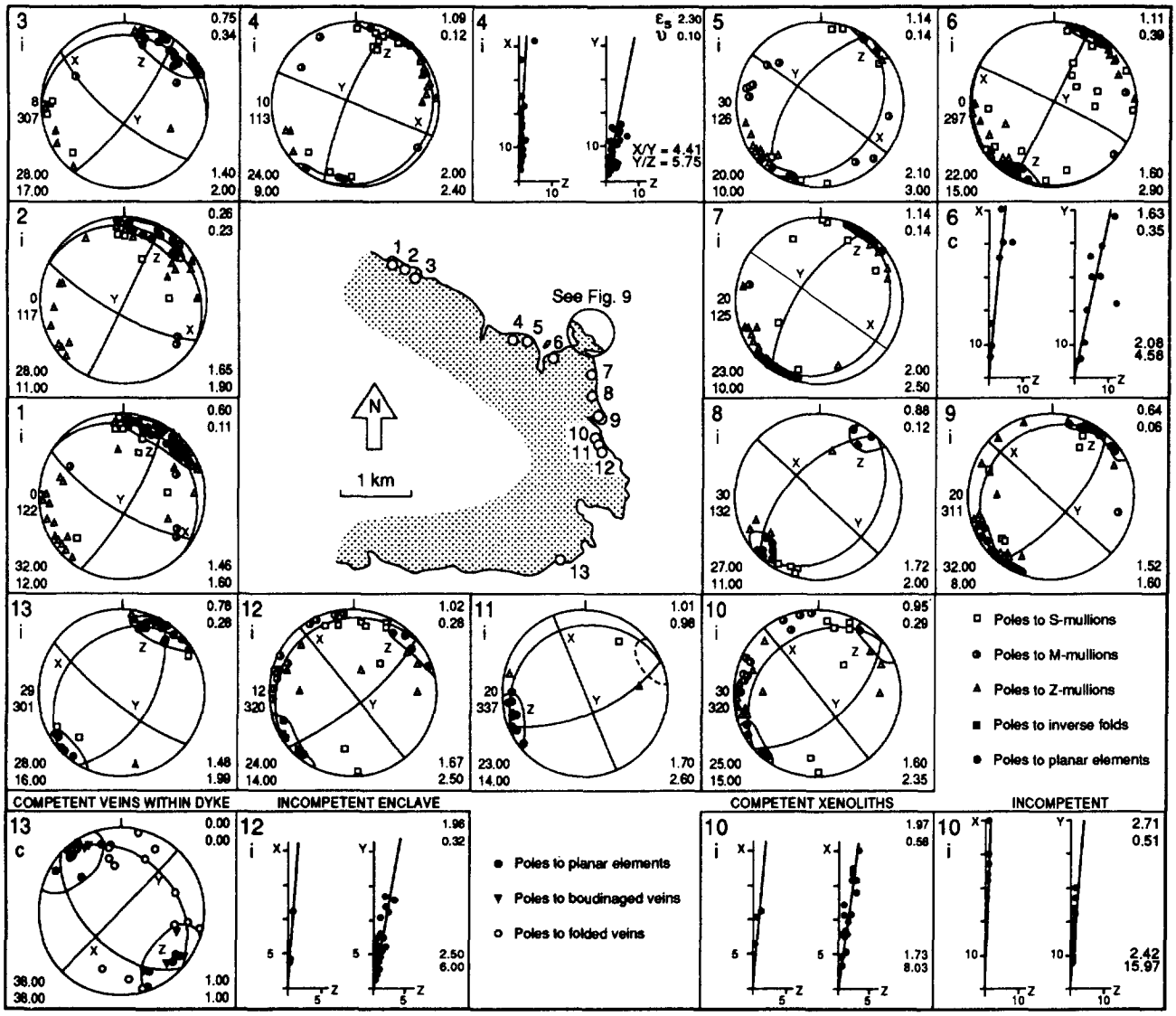

Fig. 8. Equal-area nets for dyke ellipsoids and graphs of enclave shapes for localities 1–13 shown on an outline map of the district (located on Fig. 5). Data derived by each method are distinguished by different symbols. See bottom right of Fig. 9 for key.

(or azimuth) and plunge of X; and (4) the intensity of strain as the natural logarithmic strain $\bar{\varepsilon}_s$ where

$$\bar{\varepsilon}_s = \left(\frac{2}{3}\right)^{1/2} [(\ln a)^2 + (\ln b)^2 + (\ln a \cdot \ln b)]^{1/2}$$

(Flinn 1978). (1)

The shape or anisotropy of the each ellipsoid is listed as the Lode factor, v, where

$$v = \frac{\ln b - \ln a}{\ln b + \ln a} \quad \text{(Flinn 1978).} \quad (2)$$

Measurements leading to axial ratios of the principal axes of incompetent mafic enclaves are graphed for all five localities where they could be measured in three dimensions—and for the competent granitoid xenoliths that could be measured at a single locality. The same identification numbers or symbols are used on all equal-area nets, maps, Flinn strain plots and Hsü deformation plots.

Data accuracy. The size of the ellipse of confidence depends on the accuracy of field readings and how well they constrain the axial ratios $a = X/Y$ and $b = Y/Z$ of the strain ellipsoid (Talbot 1987). Field readings constraining the *polar snoe* to accuracies of $\pm 1°$ in the planes of principal strain lead to ellipses of 95% confidence that are elongate along contours of $\bar{\varepsilon}_s$ on both logarithmic Flinn strain plots (Fig. 10) and Hsü deformation plots (Fig. 13). The ellipses of 95% confidence increase in area with increase in both $\bar{\varepsilon}_s$ and v but have lengths that only exceed twice the diameter of the data points used here for mylonites with natural logarithmic strains $\bar{\varepsilon}_s > \approx 2$.

Intensity of strain, $\bar{\varepsilon}_s$. In the Singö gneiss zone, the dykes of the Östhammer dyke swarm are characteristically decimetres to a metre wide and metres apart (Fig. 7a). Strains abruptly increase in three individual mylonite zones exposed around the coast of Hamnholm penin-

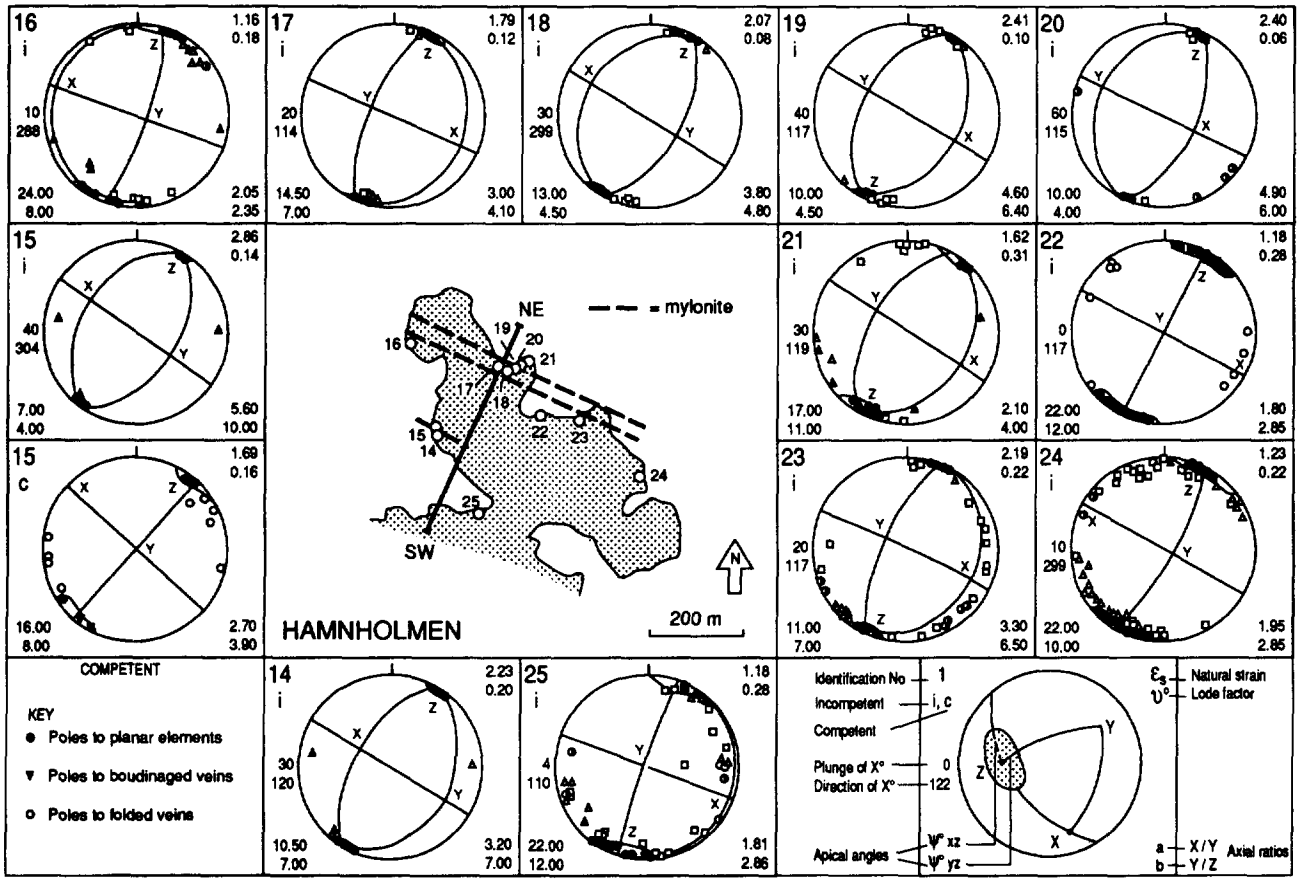

Fig. 9. Equal-area nets for dyke ellipsoids and graphs of enclave shapes at localities 14–25 on Hamnholm peninsula (located on map of Fig. 8). Dashed lines on map represent the most intense mylonites and the SW–NE line is the profile shown in Fig. 12.

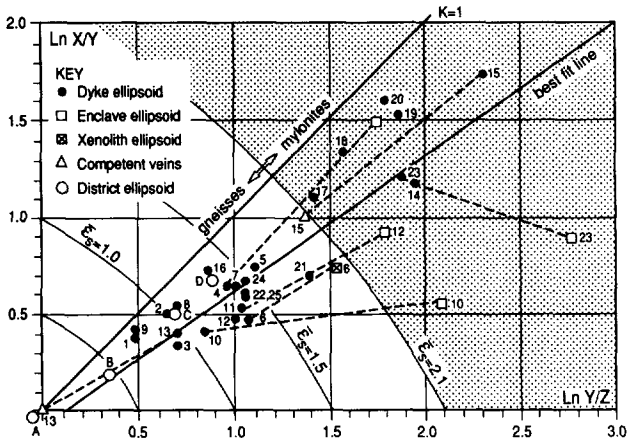

Fig. 10. Logarithmic Flinn plot of 32 ellipsoids from localities 1–25 (located on Figs. 8 and 9) throughout the district outlined on Fig. 5. Ellipsoids are constructed using incompetent dykes at 25 localities, incompetent mafic enclaves at four localities, competent granitoid xenoliths at one locality, and quartzofeldspathic veins within mafic dykes at two localities. Dashed lines connect ellipsoids constructed using different markers at the same localities. 'District ellipsoids' come from Fig. 12 (see text). Solid lines indicate the plane strain path ($v = 0$, $k = 1$) and the best fit line to all the data except for enclave outliers at localities 10 and 23.

sula. In the most northeast of these, dykes are thinned to widths and spacings of millimetres (Fig. 7b).

The distinction in the literature between gneissose, protomylonitic and mylonitic fabrics is currently qualitative and based on grain sizes and shapes and not on the intensity of their bulk strains. The macroscopic strain on which any protolith becomes a mylonite depends upon metamorphic grade and strain rate. As a result, the strain needed to mylonitize protoliths in one region cannot be exported even to similar protoliths in other regions. However, to provide the first estimate of mylonitizing strains, we compared the strains measured on scales of 2–10 m on Hamnholm peninsula (Fig. 10) with the boundaries where we (and various colleagues and visitors) agreed that granitoid protolith gneisses pass into mylonites. Our methods are capable of distinguishing the transition from gneisses to mylonites over metres (Fig. 11a) but not the transition from mylonites to ultramylonites over distances of centimetres. Nonetheless, all observers independently placed the transition where Singö gneisses with a background strain of $\bar{\varepsilon}_s \approx 1.2$ become Singö mylonites wherever detailed analysis shows the rock complex to have undergone bulk strains in excess of $\bar{\varepsilon}_s = 2.1$ (Figs. 10, 11a and 12e). *Polar snoes* in the most intense ≈3 decimetres-wide mylonites (Fig. 7b) are indeterminate by our method because all the dykes in them have been elongated. However, extrapolating our data suggests that their natural logarithmic strains exceed $\bar{\varepsilon}_s > \approx 3$ (Figs. 11a & b).

The values of $2 < \bar{\varepsilon}_s < 3$ for mylonites and $\bar{\varepsilon}_s > 3$ for ultramylonites are minima because the rock mass was already deformed before the dykes we used as strain markers were intruded. This is demonstrated by older

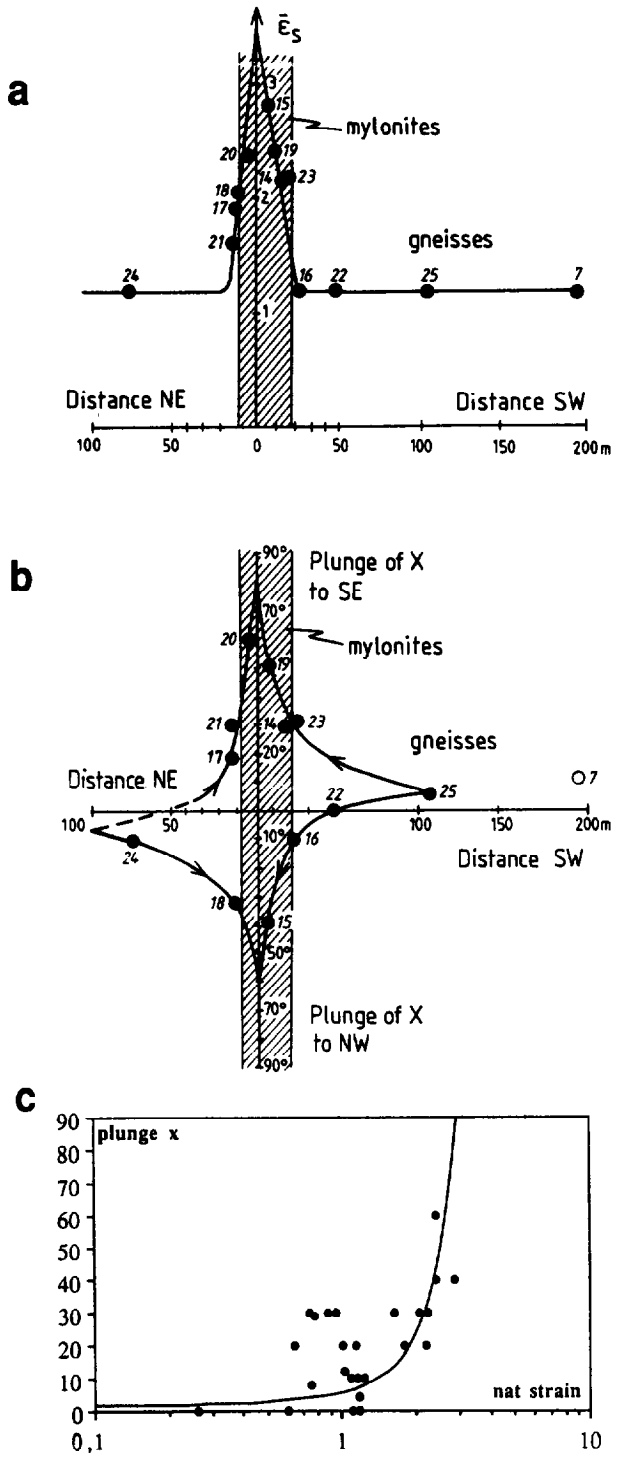

Fig. 11. (a) Natural logarithmic strains, $\bar{\varepsilon}_s$ of localities on Hamnholmen peninsula projected along strike to the profile indicated on Fig. 9 and plotted against their distance to the nearest intense mylonite. (b) Plunge of principal X axes of dyke ellipsoids on Hamnholmen peninsula plotted against cross-strike distance from the nearest intense mylonite. Plunge depends on initial attitude of X and on which side of the nearest mylonite the locality started. (c) Plunge of X axes of all 25 dykes ellipsoids in the district plotted against their natural logarithmic strains $\bar{\varepsilon}_s$. X generally steepens from near horizontal in the least deformed gneisses towards vertical in the most intense mylonites ($\bar{\varepsilon}_s > \approx 3$). The best fit curve is asymptotic with $\bar{\varepsilon}_s = 1.387*10\hat{}(0.62$ times the plunge in degrees) with $R\hat{}0.27$.

mafic enclaves and granitic xenoliths recording higher strains than dykes at the same locality (Fig. 10).

Where they are more than 40 m from the most intense mylonite, *mafic enclaves* on the northernmost spur of Hamnholm peninsula have horizontal Y/Z aspect ratios of 17:1 (mean of 26 measurements, see Figs. 6c and 9). These horizontal aspect ratios increase to 28:1 (mean of 25 readings) about 20 m from a mylonite (Figs. 6e and 9), and 260:1 (average of 19 readings) 10 m away. Similar enclaves become immeasurable streaks where their aspect ratios exceed 400:1 still metres outside strands of obvious mylonites. It is difficult to recognize such streaks as deformed enclaves until every stage in their progressive strain is seen.

Orientation with strain. In all 25 ellipsoid localities, the foliation is planar and parallel ($\pm\approx 2°$) to the XY plane of enclaves and the bulk strain ellipsoid interpreted using deformed dykes. This relation is consistent with pure irrotational bulk shear but not finite simple shear. The foliation is also axial planar to mullions in any mafic sheets (Figs. 7a & c) and buckles in granitoid screens and internal quartzo-feldspathic veins within them (Figs. 7f–h).

Although locality ellipsoids in the gneisses and mylonites are all within 30° of being coplanar, they are not colinear. The longest principal axis of strain (X) at every locality plunges gently northeast or southwest in the gneisses (e.g. Fig. 11c) and systematically steepens into the most intense mylonites (Figs. 11b and 12d). This steepening of X is only a general tendency on a simple plot of the plunge of X against $\bar{\varepsilon}_s$ in all three mylonites (Fig. 11c). However, the pattern of steepening clarifies when the plunge of X in different quadrants is related to the distance between each locality and its nearest mylonite (Fig. 11b, see also Fig. 12d). X then steepens along one of four paths depending on two factors: its pre-mylonite direction of plunge, and on which side of a mylonite the particular locality lies (Fig. 11b). The map pattern displays that the gneisses are the product of right-handed strike flow while rotated porphyroclasts (Stefan Bergmann personal communication 1991) indicate that the superposed subvertical mylonites are due to dip flow with northeast walls down (i.e. clockwise looking northwest)

Extrapolating the data (Fig. 11) suggests that X in the most intense mylonites ($\bar{\varepsilon}_s > \approx 3$) is likely to parallel the mineral orientation lineation that plunges close to 80° ESE throughout the district (Fig. 12a).

The steep mineral orientation lineation is not surprising in the dip-flow mylonites but is unexpected in the strike-flow gneisses. It is Y rather than X that subparallels the steep mineral orientation lineation in the gneisses (Figs. 12a & c). The shapes and orientations of the enclaves amongst the gneisses were inherited from deformations that preceded the Singö gneisses. Where there is sufficient vertical exposure to see them, the longest axes of the enclaves are also subvertical. The lineation in the gneisses and the enclave shapes therefore define a stretching lineation that acted as an axis of rotation rather than the direction of flow. We attribute the vertical lineation recorded by the shapes of minerals and enclaves in the gneisses to stretch by rotation during incremental strike shear with horizontal X.

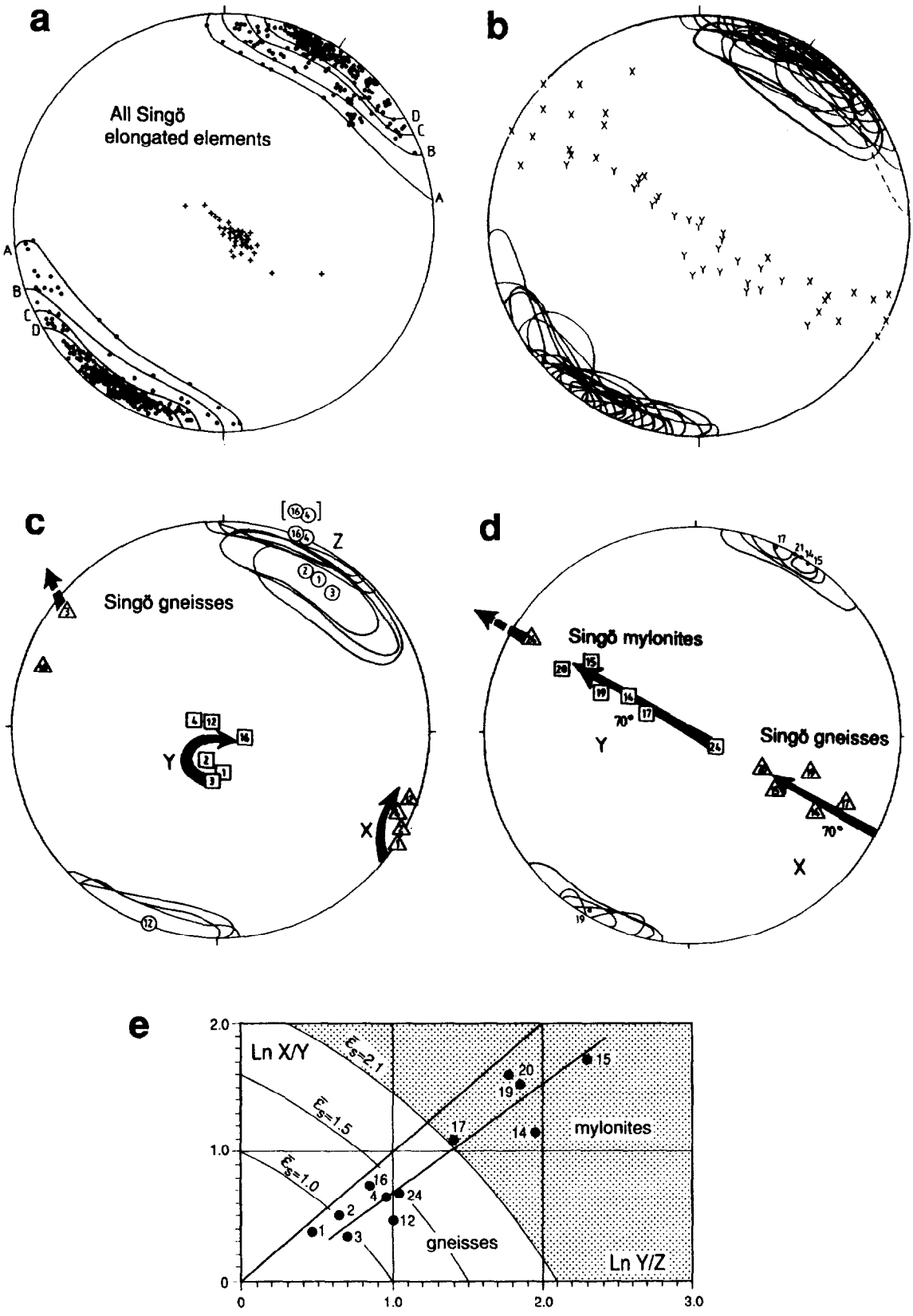

Fig. 12. Equal-area plots of (a) poles to all elongated planar elements (filled circles near periphery) and representative mineral lineations (crosses near centre) from all 25 localities in the district. Homogeneous spread of poles to elongated dyke elements show that district strain can be considered homogeneous and irrotational. Elliptical fields of overall elongation A–D enclose arbitrary values of 100%, 90%, 75% and 60% of the data. The shapes of the equivalent four district-scale 'ellipsoids' implied are plotted as open circles on Fig. 10. (b) *X* and *Y* axes and *polar snoes* for dyke ellipsoids at all 25 localities emphasize the co-axiality of Singö pure shear. This pattern contains the following details: (c) *polar snoes* in the gneisses shrank towards subhorizontal *Z* axes (numbered circles) that, like *X* (triangles) and *Y* (squares) rotated 30° clockwise around a steep axis during strike-flow. (d) *Polar snoes* for mylonites on Hamnholm peninsula shrank towards *Z* (numbered black dots) that rotated only 10° around the vertical. By contrast, mylonitization rotated *X* over 70° around *Z*, from subhorizontal in the Singö gneisses towards subvertical in the Singö mylonites. (e) A logarithmic Flinn plot shows the progressive change in shapes of the ellipsoids represented on equal-area nets (d) & (c).

Homogeneous strain on the scale of the district. Combined on the same equal-area net, poles to elongated planar dyke elements from all 25 dyke localities display a simple symmetrical concentration within a simple elliptical *polar snoe* (Fig. 12a). These are the criteria for the strain of the whole 3 × 3 km district (Fig. 8) being considered homogeneous and irrotational.

Contours enclosing 100%, 90%, 75% and 60% of the poles can be considered as district-scale fields of overall elongation (A–D on Fig. 12a) and are plotted as large open circles on the logarithmic Flinn plot (A–D on Fig. 10). The extension field enclosing 100% of the data (A on Fig.12a) indicates a homogeneous but *infinitesimal* strain of the whole 3 × 3 km district (A on Fig. 10).

Figure 12(a) demonstrates that combining data on mullions in the Östhammar dyke swarm from the entire district yields district strains that are similar but generally smaller than those in most of its constituent localities. Two potential explanations of this empirical finding are obvious (see discussion in Talbot 1987, p.130): either the dykes were being added during the strain, and/or the data from the least deformed localities control the shape and orientation of what must be considered *polar snoes* for minimum strain ellipsoids on the district scale (Fig. 12a). The second case is illustrated by the *polar snoes* for mylonitic localities (Fig. 12d) being entirely enclosed within the *polar snoes* for the district (Fig. 12a) and thus being incapable of influencing the shape or orientation of the district-scale strain ellipsoid.

Strain fields = strain paths on a logarithmic Flinn plot. All the ellipsoids constructed in the Östhammar district are plotted on Fig. 10. The vast majority of the data points fall in a simple linear strain field between $\bar{\varepsilon}_s$ values of 0 and 2.86. This field is symmetrical about a straight line fitted to all the locality ellipsoids minus two outliers. The best fit line has a gradient equivalent to $v = 0.16$ ($k = 0.7$) but intersects an ordinate at In $X/Y = 0.12$ (Fig. 10). The same line appears ato be appropriate for the district scale ellipsoids as well as all but two of the locality ellipsoids. Significantly, the exceptions are ellipsoids constructed using enclaves—a point we exploit later.

Because the sum of any two ellipsoids is always merely another ellipsoid, the shape of a single finite strain ellipsoid contains no information concerning its strain path (Ramsay 1967). However, Fig. 10 shows suites of ellipsoids recorded by four types of strain markers on different scales recording different degrees of essentially the same progressive strain in the same shear zone. District-scale ellipsoids and five of the seven dashed tielines (joining ellipsoids constructed using different markers at the same localities) all parallel the same straight line (Fig. 10). We therefore take the carefully considered risk of interpreting our linear strain *field* as indicating the strain *path* for the most deformed rocks in the district.

Linear strain paths on a logarithmic Flinn plot can result from steady stress differences driving steady irrotational strains in homogeneous materials (Ramsay 1967). That the linear strain paths on Fig. 10 included data from localities that rotated does not invalidate this concept. This is because both the locality and district scale ellipsoids (Fig. 10) record different degrees of the same strains that were irrotational on their own scales. The logarithmic Flinn plot (Fig. 10) illustrates that different localities in the Singö zone reached different distances along the same path by straining in the same manner but at different rates. However, this plot is incapable of showing that these localities also rotated within the reference frame offered by the homogeneous strain of the district (Figs. 12b & d). The strain gradient responsible for the Singö mylonites is visible as the range of $\bar{\varepsilon}_s$ on Fig. 10, but the rotational strains that occurred on scales intermediate between the localities and district are not. Exploration of this theme will be resumed after considering another problem that Ramsay (1976) presented as close to insurmountable, that of volume change.

Volume change. The shape of each of the locality ellipsoids (Fig. 10) was calculated assuming no volume change. However, if, as argued in the last section, the Singö strain *field* maps the Singö strain *path*, then that path displays the symptoms of volume loss.

Uniaxial volume loss along the Z-axis during a plane strain can change the location and/or gradient of the strain path (Hobbs *et al.* 1976, Ramsay & Wood 1976, Flinn 1978, Baker *et al.* 1993). Paths with $v = 0$ (equivalent to $k = 1$) and which intersect either axis instead of the origin of a logarithmic Flinn plot must have changed in volume at an early stage (Hobbs *et al.* 1976). Linear strain paths lying in the field of apparent flattening may have been plane strains with an early volume decrease. Linear strain paths with $v \neq 0$ (or $k \neq 1$) can therefore still represent plane strains if they developed during steady volume changes. To account for the Singö strain field intercepting the In Y/Z axis (Fig. 10), the field can be interpreted as a strain path for a plane strain with an early uniaxial volume decrease along Z of about 20% (Hobbs *et al.* 1976, see also Talbot 1987, Mazzoli 1993). A syn-shearing volumetric decrease of about 3% for each 10% total shortening along Z during a biaxial plain strain would account for the gradient of the strain path on Fig. 10 of $v = 0.16$ ($k = 0.70$).

There is some independent support for such a volume loss. The mafic sheets of the Östhammar dyke swarm comprise a larger proportion of profiles across mylonites than across their gneissose protoliths. Thus 10 mafic dykes comprise 31% of the 9 m profile across the gneisses visible in Fig. 7(a). By comparision, 23 dykes comprise 37% of a 30 cm profile across the nearby mylonites visible in Fig. 7(d). Mafic dykes therefore form 6% more of the width of this mylonite than the gneisses. The possibility that the most intense mylonites developed where the intial dilation by the dyke swarm was greatest is unlikely because few of the other equally intense mylonite strands have exceptional dyke concentrations. We therefore attribute the increase in dyke concentration to the mylonite in Fig. 7(b) having lost ≈3% volume per 10% total shortening along Z. *Mech-*

anically, the dykes were less competent so that their average widths decreased from ≈25 cm in gneisses (Fig. 7a) to 2.5 mm in the most intense mylonites (Fig. 7b), much more than the intervening granitoid screens (with average widths that narrowed from ≈50 cm in Fig. 7a to ≈7 mm in Fig. 7b). However, *chemically*, the mafic dykes were probably more competent because they had less silica and microcline to lose than their granitoid host rocks. Most of the quartz and feldspar lost from the granitoids at exposed levels probably rose to form veins at higher crustal levels but some remained to form the quartzo-feldspathic veins in some of the exposed mafic dykes (Figs. 7g & h). Point counts of thin sections confirm progressive loss of quartz and microcline with progressive mylonitisation of the granitoids (Ylva Luthander, personal communication 1994).

Locality ellipsoids in the Singö zone are interpreted here, therefore, as lying deeper in the field of apparent flattening with increasing strain because of a nearly uniaxial loss of volume at a constant rate along Z during a plane bulk shear on scales between the 2–10 m localities and the 3 × 3 km district, say 30–1000 m. Even though each of the locality ellipsoids were constructed assuming no volume change, their volumetric decrease is revealed by integrating the locality ellipsoids on the district scale (Fig. 10). Appropriate volume changes presumably occurred within each locality ellipsoid but have not been measured directly. Now that locality ellipsoids plotting in the field of apparent flattening have been attributed to shear with a steady volume decrease, the Singö deformation zone can be correctly labelled a shear zone.

Deformation path on a Hsü plot. Flinn plots (Fig. 10) can show the shape of ellipsoids but not their orientations. Although, Flinn (1978) suggested adapting his plot to show orientations, we consider that the Hsü polar plot (Owens 1974) is more appropriate because it has strain fields that are equal in size for ellipsoids having equivalent shapes but different orientations (Talbot *et al.* 1987, Mazzoli 1993). Volume changes can be indicated on a Hsü plot by moving the centre point (Owens 1974).

This section explores the implications of the X axes of the locality ellipsoids steepening from sub-horizontal in the Singö gneisses to sub-vertical in the superposed Singö mylonites (Figs. 12b & d) even though the mineral lineation remains consistently steep (Fig. 12a). To do this, the locality ellipsoids shown on the logarithmic Flinn plots (Fig. 10) are repeated in part of a Hsü plot so that the orientations of locality ellipsoids are related to the strain axes of the district (Fig. 13a). Most previous workers have used only a single 60° arc of a polar plot to show ellipsoid shapes independently of their orientation. But this use squanders the full potential of the Hsü plot. Rather than being just another version of a Flinn strain plot, Fig. 13(a) is instead a deformation plot. It combines the information on the symmetries and intensities of strains shown on Fig. 10 with their rotation with increasing strain shown on Figs. 11 and 12. Figure 13(a) shows the deformation of *locality* ellipsoids in the context of the spatial coordinates of the *district* (Fig. 12a).

The full Hsü polar diagram is divided into six 60° segments bound by three orthogonal spatial axes, **H**, **L** and **V** defined relative to the regional tectonic grain as proposed indirectly by Harland & Bayly (1958). **V** is vertical, **H** is horizontal and perpendicular to the regional foliation and **L** is parallel to the strike of the regional foliation. Each 60° segment is equivalent to a Flinn diagram in that all possible ellipsoids may be shown uniquely if they have appropriate coaxial or coplanar orientations (indicated by the peripheral diagrams around Fig. 13a). The segments shown here represent ellipsoids with vertical XY planes (and foliations) that strike NW–SE and SW–NE.

The most obvious use of the Hsü plot is for analyzing ductile co-axial homogeneous strains (e.g. Talbot *et al.* 1987) but here, part of it is adapted to show coplanar but non-coaxial strains (Figs. 12 d–e). This is done by ignoring differences of up to 30° in the orientation of the foliation (and Z) from one locality to another (Figs. 12b–d). Thus we assume that the XY planes for all locality ellipsoids are vertical and parallel to the mylonitic foliation on Hamnholmen peninsula with its strike of 122° from north (Fig. 12d).

Strain ellipsoids representing the least deformed gneisses, the most deformed mylonites and the enclaves appear in different parts of the Hsü plot (Fig. 13a) because their principal strain axes have different orientations with respect to the regional strain axes **H**, **L** and **V**. Thus the X axes of the least deformed gneisses are horizontal (Figs. 11b–c and 12 c–d) whereas the X axes in the enclaves and the most intense mylonites are close to vertical. Dyke ellipsoids at every locality are shown in Fig. 13(a) with $\bar{\varepsilon}_s$ plotted along the radials and the plunges of their X axes (listed on Figs. 8 and 9 and illustrated on Figs. 11c and 12c–d) plotted around the outer circumference.

The advantage of Fig. 13(a) becomes clear when the strain *field* for the district (Fig. 10) is reconsidered assuming it to be the strain *path* for the most deformed mylonites in that district. The linear *strain* path on Fig. 10 shows only the shapes and intensity of locality strains; the curved *deformation* path on Fig. 13(a) (imported from Fig. 11c) also shows the rotation of the X axes of the locality ellipsoids in the context of the Singö zone as a whole.

The path fitting the data in Figs. 11(c) and 13(a) curves progressively from the $v = 0$ ($k = 1$) radial in gneisses due to strike flow, to the $v = 0$ ($k = 1$) radial in the dip-flow mylonites at $\bar{\varepsilon}_s \approx 3$ (actually nearer $v = 0.16$ or $k \approx 0.7$ because of the progressive volume decrease). This path passes through the *district* scale plane of uniaxial flattening ($v = 1$ along the **H** radial) and (because the distal end of the path parallels the **−V** radial) indicates that the highest finite strains result from final incremental strains that were vertical constrictive.

Ellipsoids on both sides of the **H** radial (Fig. 13a) only retained similar shapes on the locality scale (Fig. 10) because they rotated in the context of the district. The

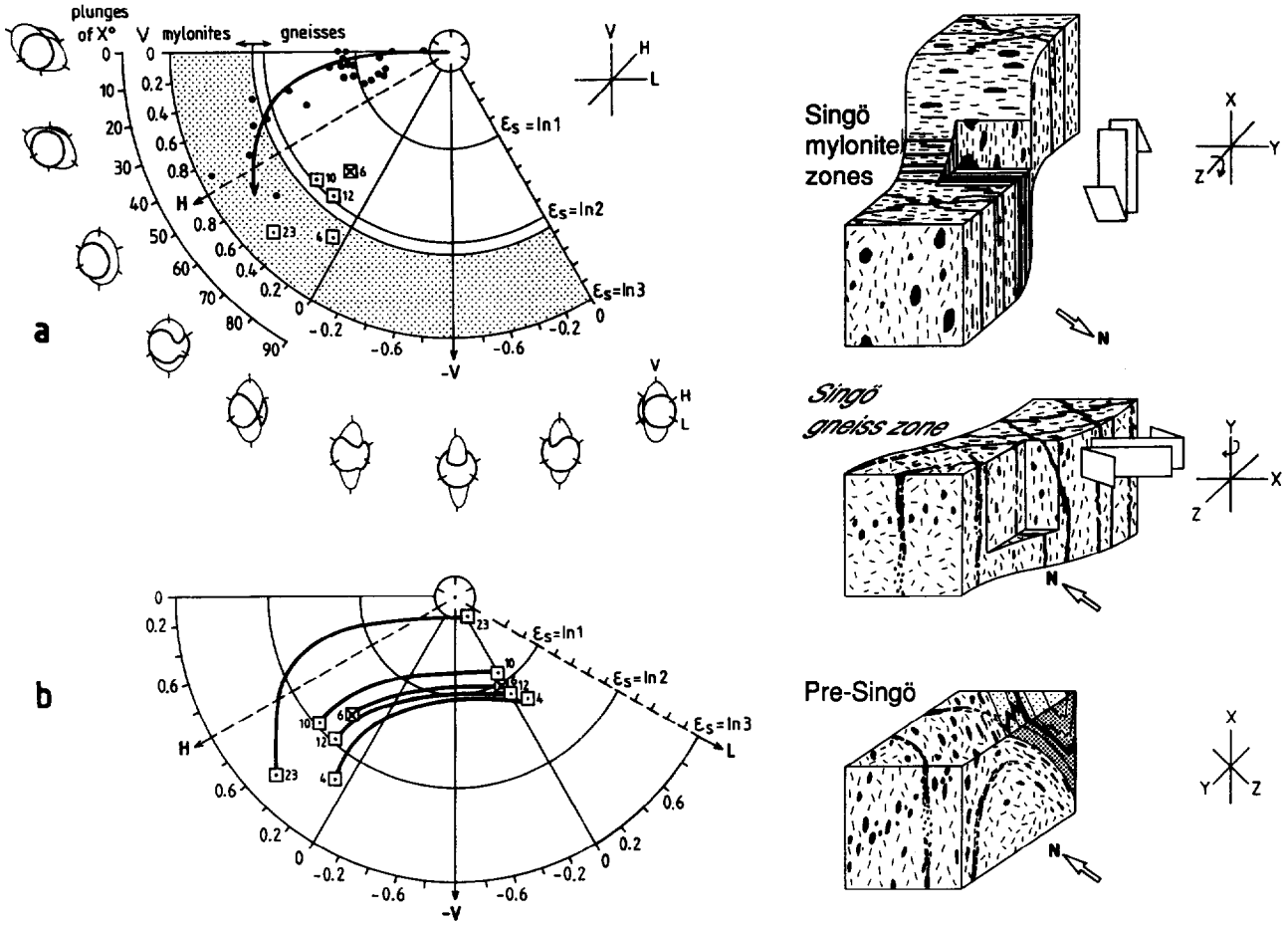

Fig. 13. Block diagrams cartoon three stages in the deformation history of the district recovered on the partial Hsü deformation plots on the left. Notice different orientations of blocks relative to North. (a) Dyke ellipsoids at every locality (black dots) are plotted using their $\bar{\varepsilon}_s$ along radials and the plunge of their X axes around the *outer* circumferential scale. The $\bar{\varepsilon}_s = 2.1$ contour divides mylonites from gneisses in the Östhammar area. Enclave ellipsoids (squares) are plotted with $\bar{\varepsilon}_s$ along radials and v around the *inner* circumferential scale (see peripheral diagrams). All locality ellipsoids are related to the same district-scale strain axes (**H**, **L** and **V** arranged as on insert in a). The deformation path for the district is shown for the most deformed mylonites and is the regional expression of the strain paths fitting data in Figs. 10 and 11(c). (b) Removing the effects of the Singö mylonites from each of the five enclave ellipsoids (by removing that part of the regional deformation path with the same $\bar{\varepsilon}_s$) reveals that the enclaves were plane strained on a vertical NE-trending plane before the Singö shear zone developed.

deformation path on Fig. 13(a) indicates that gneisses passed through an incremental phase where they flattened uniaxially in the vertical plane striking-NW before some of them began to mylonitize by shearing vertically in the same plane.

Perhaps the greatest advantage of the Hsü plot is that it is a vector space so that strains shown on it can easily be manipulated graphically. Successive strains superposed one on another can be removed in reverse order by geometric vector subtraction (Talbot *et al.* 1987). Appropriate segments of the district scale deformation path determined from the dyke ellipsoids (Fig. 13a) can be removed from the enclave ellipsoids. This has been done (Fig. 13b) by removing from each of the enclave ellipsoids that part of the deformation path of the district with the same natural strain ($\bar{\varepsilon}_s$). This procedure reveals that the enclaves occupied a linear deformation field before the Singö gneisses and mylonites were superposed. This linear field was along the radial $v = 0$ (midway between the **−V** and **L** radials on Fig. 13b). It indicates that, before they were further distorted by the Singö shear zone, the enclaves were already deformed to $\bar{\varepsilon}_s \approx 1$ (gneisses?) with subvertical X axes close to a plain shear with a vertical NE-trending XY plane.

Stålhös (1984, 1991) synthesized the tectonic history of the supracrustal rocks in the Svecofennian terrain that includes Östhammar. He distinguished two main tectonic phases after the emplacement of the granitoid plutons. The supracrustal rocks were first folded into recumbent folds which verged westward about generally north–south axes before they were refolded about upright EW-trending folds. If the late west-northwest–east-southeast grain of the Singö shear zone can be equated with the generally east–west late tectonic grain of the region, then the steep NE-striking plain strain inferred to have preceded the Singö shear zone near Östhammar (Fig. 13b) could be equivalent to Stålhös' earlier phase of post-plutonic deformation.

DISCUSSION AND SYNTHESIS OF REGIONAL TECTONIC HISTORY

Like the Svecofennian sialic crust in most of Fennoscandia, the Östhammar region was built by granitoid plutons intruding their own volcanics in magmatic arcs diluted by shelf carbonates, cherts and clastic sediments. Basaltic magmas were pumped from the mantle through this complex crust as it was being built. Early mantle melts were incorporated into the granitoids, first by magma mingling and then by migma–magma mixing when mafic dykes were dispersed as enclaves amongst aplitic melts generated by the dykes themselves. The enclaves are the Cheshire-Cat-like grins of former dykes that fed the mafic volcanics interlayered among the rhyolites (Figs. 6a & b).

As the region cooled, further intrusions of mantle magmas survived as the Östhammar dyke swarm. The primary en échelon shapes of the two conjugate sets of these dykes indicate deep emplacement (Roberts 1970, Nicholson & Pollard 1985). Pulses in magma pressure dilated conjugate shears induced by a stress field which temporarily exceeded the minimum and intermediate principal axes of the stress field likely to have been responsible for the subvertical WNW-foliation in the Singö gneiss zone. Both the early enclaves and the later dykes have been shown to be potent strain markers despite having been incompetent.

The ductile story of the Singö zone involved progressive increments of plane strain in three regimes; all had principal strains orthogonal to the zone, but the labels on each axis were different at each stage. Thus the X and Z axes swapped and the X and Y rotated about a Z axis perpendicular to the zone. This story explains how both the Singö gneisses, their enclaves, and the Singö mylonites all share the same subvertical mineral orientation lineation. This stretching lineation was the flow direction in the mylonites but, in an environment where metabasaltic sheets deformed faster than their granitoid host rocks, was the rotation axis for the shear in their protolith gneisses. Strike flow in the gneisses and the rotational nature of their stretching lineation are cryptic and would not have been suspected had we not analyzed their homogeneous bulk strains.

The first shear in the district left the enclaves with subvertical X axes in gneisses with a vertical XY plane trending-NE. Soon after that, the Östhammar dykes were intruded in a NW-trending wrench regime (at ≈1.86 Ga). Their subsequent ductile strain recorded a right-handed transpression (≈1.86–1.83 Ga) in which a uniaxial volume loss occurred during a pure biaxial shear. Additional increments of this strike-flow distorted the finite shapes of the enclaves through a vertical prolate fabric towards the horizontal.

There are surprisingly few signs of rotation within the Singö shear zone—and those few are all around unexpected axes. Instead of *polar snoes* sweeping across the equal-area net as X and Z rotated about Y as expected of simple shear, the *polar snoes* closed about stationary Z axes that are generally orthogonal rather than oblique to the Singö zone (Figs. 12a–d). Together with planar foliations and enclave shapes paralleling the bulk XY plane, these relationships indicate pure irrotational rather than simple rotational shears. The current San Andreas fault also appears to involve pure rather than simple shear (Evans & Wong 1992). Refraction of principal stresses so that they are orthogonal to the San Andreas fault is attributed to high pore-fluid pressures in already weak fault gouges at surficial crustal levels. Perhaps stress refraction at deeper levels in the Singö shear zone occurred in gneisses in strain-rate softening because of high pore-fluid pressures indicated by their volume decrease as they mylonitized.

Despite all the locality ellipsoids being constructed assuming none, volume loss becomes obvious on the Flinn strain plot. We attribute apparent flattening in the Singö shear zone to both the gneisses and mylonites having undergone steady syn-shearing volume decreases of ≈3% for every 10% total shortening of Z by what otherwise would have been pure shears. This volume decrease can be blamed on the uniaxial loss of quartz and microcline along the axis of shortening in chemically incompetent granitoids. Some of this loss is probably represented by the quartzo-feldspathic veins in the mechanically incompetent mafic dykes. Gneissose fabrics in granitoid protoliths with $\bar{\varepsilon}_s = 1.2$ became mylonites at $\bar{\varepsilon}_s = 2.1$ and ultramylonites at $\bar{\varepsilon}_s > \approx 3$.

Deformation ellipsoids constructed using four types of strain markers on both locality and district scales share the same linear strain field on a logarithmic Flinn plot. This strain field was interpreted as the strain path and converted to a deformation path by replotting it taking account of approximate orientations on a Hsü plot. Removing increments of plane strain recorded in the Singö gneiss and mylonite zones revealed axial swapping between three phases of shear. The interpretation that the enclaves were plane strained with subvertical X axes in a subvertical northeast plane before the dyke swarm was emplaced agrees with an earlier analysis of a much larger region south of the Singö zone by Stålhös (1984, 1991).

Previous studies of Proterozoic Sweden have shown how the foliations inherited from crustal construction were penetrative on regional scales until strain began to localise in gneiss zones only a few kilometres wide (e.g. Talbot *et al.* 1989, Talbot & Heeroma 1989, Munier & Talbot 1993). Like the Singö zone, many other such gneiss zones narrowed through mylonites tens of metres wide to seismic faults only millimetres wide as the rocks now exposed rose through the greenschist metamorphic facies. As each rock mass was uplifted further, it cooled, cratonised, and became increasingly brittle. Subsequent reactivations jostled the craton along formerly ductile shear zones that widened to zones of brittle veins and fractures along slickenlined faults (Munier & Talbot 1993).

This is the first study to demonstrate that dip-flow mylonites anastomose among co-planar gneisses due to a preceding stage of cryptic transpression. Transpression leads to a space problem. Rocks between zones of

transpression can extrude laterally (as China is being extruded into the open Pacific) and/or extrude vertically up, out and over a foreland basin as piles of orogenic nappes. The Singö zone may have done both. Early transpression in the Singö gneisses (≈1.86–1.83 Ga) led to progressive strike-flow until X steepened in narrowing mylonites with biaxial dip-flow so that intervening lenses of gneiss extruded vertically (≈1.83–1.60 Ga). Perhaps the Singö shear zone accommodated lateral extrusion before an ocean closed and it became the root zone of a former pile of nappes extruded from the suture.

> Alice (in Wonderland, on the way through the Looking Glass) a little timidly:
> "which way ought I to go from here?"
> Cheshire-Cat: "That depends a good deal on where you want to get to."
>
> (Carroll 1865)

Acknowledgements—We thank Göran Stålhös for directing us to three areas in eastern Sweden with well exposed deformed incompetent mafic inclusions. We chose the coast near Östhammar because the sheets there are more numerous, better exposed and record a simpler strain history than elsewhere (where younger mullions remullion older mullions). We thank Ylva Luthander for having analyzed the thin sections. We are also grateful to many other colleagues for discussion, in particular to Iain Allison and an anonymous referee for helping improve earlier versions of the manuscript. Christina Wernström and Lill Wahlund are thanked for drafting most of the figures. The research reported here was part of DS's Ph.D. thesis which was supported by an Uppsala University research studentship. CJT wrote the final version while on sabbatical at the Geophysical Laboratory of the Carnegie Institution of Washington.

REFERENCES

Allaart, J. H. 1967. Basic and intermediate igneous activity and its evolution in the Julianhåb Granite, South Greenland. *Meddr. Grønland* **175**, 1–136.

BABEL working group 1993. Integrated seismic studies of the Bothnian shield using data in the Gulf of Bothnia region. *Geophys. J. Int.* **112**, 305–324.

Baker D. W., Chawla, K. S. & Kriezek, R. J. 1993. Compaction fabrics of pelites: experimental consolidation of kaolinite and implications for analysis of strain in slate. *J. Struct. Geol.* **15**, 1123–1137.

Becker, G. F. 1893. Finite homogeneous strain, flow and rupture of rock. *Bull. geol. Soc. Am.* **4**, 13–90.

Berger, A. R. 1971. Dynamic analysis using dykes with oblique internal foliations. *Bull. geol. Soc. Am.* **82**, 781–786.

Båk, J., Sorensen, K., Grocott, J., Kortsgård, J. A., Nash, D. & Watterson, J. 1975. Tectonic implications of Precambrian shear belts in western Greenland. *Nature* **254**, 566–569.

Carlsson, A. & Christiansson, R. 1986. Rock stresses and geological structures in the Forsmark area. *Proc. Int. Symp. Rock Stress & Rock Stress Measurements*. Stockholm, 1–3 September 1986.

Carroll, L. 1865. *Alice's Adventures in Wonderland*. (e.g. pp. 62–65 of *The Complete Illustrated Works of Lewis Carroll*, Chancellor Press, London, 1989.)

Cruden, A. R. 1990. Flow and fabric development during the diapiric rise of magma. *J. Geol.* **98**, 681–698.

Davidson, L. M. & Park, R. G. 1978. Late Nagssugtoqidian stress orientations derived from granodioritic dykes north of Hosteinsborg, West Greenland. *J. geol. Soc. Lond.* **135**, 238–239.

De Sitter, L. U. 1958. Boudins and parasitic folds in relation to cleavage and folding. *Geol. Mijnb.* **20**, 277–286.

Ehlers, C., Lindroos, A. & Selonen O. 1993. The late Svecofennian granite–migmatite zone of southern Finland—a belt of transpressive deformation and granite emplacement. *Precambrian Res.* **64**, 295–309.

Ekman, M. 1991. Gravity change, geoid change and remaining postglacial uplift of Fennoscandia. *Terra Nova* **3**, 390–392.

Eriksson, L. & Henkel, H. 1988. Storstrukturella zoner in Forsmarksområdet. SGU geofysiskrappart BRAP 88402.

Evans, B. & Wong, T-F. (Eds) 1992. *Fault Mechanics and Transport Properties of Rocks*. Academic Press, New York.

Flinn, D. 1962. On folding during three-dimensional progressive deformation. *Q. Jl. geol. Soc. Lond.* **118**, 385–428.

Flinn, D. 1978. Construction and computation in three-dimensional progressive deformations. *Q. Jl. geol. Soc. Lond.* **135**, 291–305.

Fletcher, R. C. 1982. Analysis on the flow in layered fluids at a small, but finite, amplitude with application to mullion structures. *Tectonophysics* **81**, 51–56.

Gaal, G. & Gorbatschev, R. 1987. An outline of the Precambrian evolution of the Baltic Shield. *Precambrian Res.* **35**, 15–52.

Gay, N. C. 1968. The motion of rigid particles embedded in a viscous fluid during pure shear deformation of the fluid. *Tectonophysics* **3**, 81–88.

Ghosh, S. K. 1966. Experimental tests of buckling folds in relation to the strain ellipsoid in simple shear deformations. *Tectonophysics* **3**, 169–185.

Gorbatschev, R. & Bogdanova, S. 1993. Frontiers in the Baltic shield. *Precambrian Res.* **64**, 3–21.

Harland, W. B. & Bayly, M. B. 1958. Tectonic regimes. *Geol. Mag.* **45**, 89–104.

Henkel, H. 1991. Magnetic crustal structures in northern Fennoscandia. *Tectonophysics* **192**, 57–79.

Hobbs, B. E., Means, W. D. & Williams, P. E. 1976. *An Outline of Structural Geology*. Wiley, New York.

Holst, N. O. 1887. Beskrifning till Kartbladet Svartklubben. *Sveri. geol. Unders.* **Af 97**.

Hossack, J. R. 1968. Pebble deformation and thrusting in Bygdin area (southern Norway). *Tectonophysics* **5**, 315–339.

Huppert, H. E. & Sparks, R. J. S. 1988. Generation of siliceous magma by heat transfer from basaltic sills intruded into lower crust. *J. Petrol.* **29**, 599–624.

Hutton, D. H. W. 1982. A tectonic model for the emplacement of the Main Donegal granite, NW Ireland. *Q. Jl. geol. Soc. Lond.* **169**, 615–631.

Jackson, M. P. A. & Robertson, D. I. 1983. Regional implications of early-Precambrian strains in the Onverwacht Group adjacent to the Locheil Granite, northwest Swaziland. In: *Contributions to Geology of the Barberton Mountain Land* (edited by Anhaeusser, C. R.). *Spec. Publ. geol. Soc. South Afr.* **9**, 45–62.

Johnson, M. R. W. & Dalziel, I. W. D. 1966. Metamorphosed lamprophyres and late thermal history of the Moines. *Geol. Mag.* **103**, 240–249.

Julian, B. R., Miller, A. D. & Foulger, G. R. 1993. Non-shear focal mechanisms of earthquakes at the Geysers, California, and Hengill, Iceland, geothermal areas. *Proc. Geotherm. Res. Council* **17**, 123–128.

Kaitero, S. 1953. Geological structure of the late Precambrian intrusives of the Åva area, Åland islands. *Bull. Comm. Geol. Finland* **162**, 4–79.

Law, A. 1994. Novel uses of high-density pre-clinical seismic reflection data from the Baltic Shield. Unpublished Ph.D. Thesis. BIRPS, Cambridge University.

Lundqvist, T. 1979. The Precambrian of Sweden. *Sver. Geol. Unders.* **C 768**.

Mandal, N., Khan, D. & Deb, S. K. 1992 An experimental approach to wide-necked pinch and swell structures. *J. Struct. Geol.* **14**, 395–403.

Mazzoli, S. 1993. A graphical representation of coaxial plane strains and volume changes. *J. Struct. Geol.* **15**, 939–942.

Mehnert, K. R. 1968. *Migmatites and The Origin of Granitic Rocks*. Elsevier, Amsterdam.

Munier, R. & Talbot, C. J. 1993. Segmentation, fragmentation and jostling of the cratonic basement in and near Äspö, southeast Sweden. *Tectonics* **12**, 713–727.

Nicholson, R. & Pollard, D. D. 1985. Dilation and linkage of echelon cracks. *J. Struct. Geol.* **7**, 583–590.

Owens, W. H. 1974. Representation of finite strain state by three axis planar diagrams. *Bull. geol. Soc. Am.* **85**, 307–310.

Passchier, C. W. 1990a. A Mohr construction to plot the stretch history of material lines. *J. Struct. Geol.* **12**, 513–515.

Passchier, C. W. 1990b. Reconstruction of deformation and flow parameters from deformed vein sets. *Tectonophysics* **180**, 185–199.

Passchier, C. W., Myers, J. S. & Kröner, A. 1990. *Field Geology of High-Grade Terrains*. Springer-Verlag, Berlin.

Passchier, C. W. & Sokoutis, D. 1993. Experimental modelling of mantled porphyroclasts. *J. Struct. Geol.* **15**, 895–909.
Pitcher, W. S. & Berger, A. R. 1972. *The Geology of Donegal*, Wiley Interscience, London.
Ramberg, H. 1963. Strain distribution and geometry of folds. *Bull. geol. Instn. Univ. Uppsala.* **47**, 484–505.
Ramsay, J. G. 1967. *Folding and Fracturing of Rocks*. McGraw-Hill, New York.
Ramsay, J. G. 1976. Displacement and strain. *Phil. Trans. R. Soc. Lond.* **A188**, 3–25.
Ramsay, J. G. & Wood, D. S. 1976. The geometric effects of volume changes during deformation processes. *Tectonophysics* **16**, 263–277.
Ramsay, J. G. & Huber, M. I. 1983. *The Techniques of Modern Structural Geology. Vol.* 1, *Strain Analysis*. Academic Press, London.
Roberts, J. L. 1970. The intrusion of magma into brittle rocks. In: *Mechanism of Igneous Intrusions* (edited by Newall, G. & Rast, N.). Gallery Press, Liverpool, 283–338.
Sederholm, J. J. 1932. On the geology of Fennoscandia. *Bull. Comm. Geol. Finland* **98**, 1–30.
Sellés-Martinez, J. 1993. A common misinterpretation of the equal-area net properties. *J. Struct. Geol.* **15**, 1361–1413.
Sjöström, H. & Bergman, S. 1993. The tectonometamorphic history of a major shear zone in central Sweden—integrated geological-geophysical studies. Sveriges Geologiska Undersökning, Rapporter och meddelandernan No. 76, page 17.
Smith, D. I. 1979. Caledonian minor intrusions of the N. Highlands of Scotland. *J. geol. Soc. Lond.* **134**, 414.
Smith, R. B. 1975. Unified theory on the onset of folding, boudinage, and mullion structure. *Bull. geol. Soc. Am.* **86**, 1601–1609.
Smith, R. B. 1977. Formation of folds, boudinage, and mullions in non-Newtonian materials. *Bull. geol. Soc. Am.* **88**, 312–320.
Sokoutis, D. 1987. Finite strain effects in experimental mullions. *J. Struct. Geol.* **9**, 233–242.
Sokoutis, D. 1990. Experimental mullions in single and double interfaces. *J. Struct. Geol.* **12**, 365–373.
Stålhös, G. 1984. Svecokarelian folding and interfering macrostructures in eastern Central Sweden. In: *Precambrian Structures Illustrated* (edited by Kröner, A. & Greiling, R.). E. Schweizerbart'sche Verlagsbuchhandlung, Stuttgart, 369–379.
Stålhös, G. 1991. Beskrivning till berggrundskartorna Östhammare NV, NO, SV, SO. (1:50,000 bedrock maps and description with English summary) Sveriges. Geologiska Undersökning, Series Af.
Talbot, C. J. 1970. The minimum strain ellipsoid using deformed quartz veins. *Tectonophysics* **9**, 47–76.
Talbot, C. J. 1982. Oblique foliated dykes as deformed incompetent single layers. *Bull. geol. Soc. Am.* **93**, 450–460.
Talbot, C. J. 1983. Microdiorite sheet intrusions as incompetent time- and strain markers in the Moine assemblage NW of Great Glen fault, Scotland. *Trans. R. Soc. Edinb.* **74**, 137–152.
Talbot, C. J. 1987. Strains and vorticity beneath a tabular batholith in the Zambesi belt, Zimbabwe. *Tectonophysics* **138**, 121–158.
Talbot, C. J. & Sokoutis, D. 1988. The Singö shear zone near Östhammar, Univ. Uppsala Dept. Min. & Pet. Research report No 55.
Talbot, C. J. & Heeroma, P. 1989. Cover/basement relationships in the SW Swedish gneisses near Varberg. *Geol. Fören. Stockholm. Förhand.* **111**, 105–119.
Talbot, C. J. & Sokoutis, D. 1992. The importance of incompetence. *Geology* **20**, 951–953.
Talbot, C. J., Hunter, D. R. & Allen, A. R. 1987. Deformation of the Assegai supracrustals and adjoining granitoids, Transvaal, S. Africa. *J. Struct. Geol.* **9**, 1–12.
Talbot, C. J., Riad, L. & Munier, R. 1989. Reactivation of Proterozoic shear zones. In: *Interdisciplinary Study of Post-glacial Faulting in the Lansjärv Area, N Sweden* (edited by Bäckblöm, G. & Stanfors, R.). SKB Technical Report **89–31**.
Tirén, S. A. 1991. Geological setting and deformation history of a low angle fracture zone at Finnsjön, Sweden. *J. Hydrol.* **126**, 17–44.
Treagus, S. H. & Sokoutis, D. 1992. Laboratory modelling of strain variation across rheological boundaries. *J. Struct. Geol.* **14**, 405–424.
Vernon, R. H. 1984. Microgranitoid enclaves in granite–globules of hybrid magma quenched in a plutonic environment. *Nature* **309**, 438–439.
Von Brunn, V. & Talbot, C. J. 1986. Formation and deformation of sub-glacial intrusive clastic sheets in the Dwyka Formation of Northern Natal, South Africa. *J. Sed. Petrol.* **56**, 35–44.
Watterson, J. S. 1968. Plutonic development of the Itordleq area, South Greenland, Part 111: Late kinematic basic dikes. *Meddr. Grønland* **185**, 1–104.
Weijermars, R. 1993. Progressive deformation of single layers under constantly orientated boundary stresses. *J. Struct. Geol.* **14**, 911–922.
Welin, E., Kähr, A.-M. & Lundegårdh, P. H. 1980. Rb–Sr isotope systematics at amphibolite facies conditions, Uppsala region, eastern Sweden. *Precambrian Res.* **13**, 87–101.
Welin, E. & Stålhös, G. 1986. Maximum age of the synmetamorphic Svecokarelian fold phases in south central Sweden. *Geol. Fören. Stockholm. Förhand.* **108**, 31–34.
Wilson, G. 1961. The tectonic significance of small-scale structures and their importance to the geologist in the field. *Annals. Soc. géol. Belg.* **84**, 510–517.

APPENDIX

Introduction

The main text describes bulk strains measured by mapping their *polar snoes*. Here we add some incidental findings about inhomogeneous strains on the scale of decimetres of the incompetent dykes that we used as strain markers.

These findings are presented in terms of a discussion of an old problem: that the sum of two ellipsoids is merely a third ellipsoid (Ramsay 1967, see also Ramsay & Huber 1983). Part of Ramsay's lesson that strain ellipsoids cannot record their strain paths was that pure and simple shears cannot be distinguished because the resulting ellipsoids are identical in shape. We accept that the *shape* of a strain ellipsoid contains no information about whether or not it has spun—but still circumnavigate this problem by two routes. In the main text we distinguish rotations of individual locality ellipsoids by comparing their magnitudes and orientations within the natural reference frames provided by the mylonites and their foliation (Fig. 12 and later). Spin of localities are represented there by the X axes rotating within the foliation. Here we ask if spin can be seen within the localities themselves using vorticity recorded in the shapes and orientations, not of the bulk ellipsoids, but of strain-active markers within them.

We ask this question because early speculation over whether bulk rotations can be recognized using complications in the structural histories of strain markers (De Sitter 1958, Flinn 1962, Ramsay 1967, Talbot 1970) have recently been revived (e.g. Passchier 1990a,b, Weijermars 1993). Thus Passchier suggested using the symmetry histories of internal structures to distinguish whether a locality has spun or not. In essence, a bulk strain has spun if the sum of its internal vorticities is asymmetric. This route requires understanding a special case of the *polar snoe*: the polar surface of no *infinitesimal* elongation.

This Appendix therefore opens with brief reminders of how we read the signs of vorticity in rocks and a definition of the *polar snoie*. We then explain why it is not as easy as expected to map the infinitesimal *polar snoie* but easier than expected to map the finite *polar snoe*. Both the difficulty of mapping the *polar snoie* and the relative ease of mapping the *polar snoe* remind us that rocks do not read the literature and do not indulge in all the potential complications expected of them.

1. *Can we recognize incremental strains directly?*

1.1. *Symmetry and vorticity*. Unlike homogeneous strain ellipsoids, strain-active material markers have partial memories of the inhomogeneous strains they have suffered—and we can read at least the sign of their vorticity (clockwise or counterclockwise). Thus trails around isolated competent inclusions exhibit left- or right-handed sigma, delta or theta shapes ± stairstepping (Passchier & Sokoutis 1993). Similarly, most single layers are expected to record the sign of their vorticity by the s, z, or m symmetries of any structures or fabrics they develop. This is not always so, few of the thousands of buckles and pinches measured by Talbot (1987) were particulary asymmetric. By contrast, many of the mullions used in this work are strongly asymmetric. Indeed, we were relieved to find that we had little difficulty in distinguishing primary bridges and bayonets from secondary mullions even after strong bulk strains (Figs. 6e–g).

1.2. *The infinitesimal snoie and polar snoie*. The surface of *no* infinitesimal elongation (and the surface traced by poles to it) are special cases of the *snoe* and *polar snoe*. The *snoie* joins the line of intersection between an infinitesimal strain ellipsoid and its initial sphere with their common centre. The *polar snoie* is another set of elliptical cones traced by poles to the *snoie*.

The surface of no infinitesimal elongation (*snoie*) is sought by seismologists who derive earthquake solutions. Until recently, seismology was simplified by assuming that all earthquakes involved only simple (biaxial) shear in which the *snoie* decomposes into two focal planes at right angles. It is now being appreciated that, for earthquakes due to triaxial strains, dilational and compressional first P-wave arrivals arrive either side of a conical *snoie* with the apical angle indicated along the topmost curve in Fig. 4 (e.g. Julian *et al.* 1993).

1.3. *Do structural complications allow direct mapping of the polar snoie?* Material lines and planes (and poles to planes) not lying in the principal planes of shears rotate during progressive bulk strains. Material planar markers which start with poles just outside the *polar snoie* begin their deformation history by decreasing in area (and either buckling or mullioning: Flinn 1962, Weijermars 1993). As their poles rotate through the *polar snoie* the planes increase in area and reach their initial area as their poles rotate through the *polar snoe*; thereafter they increase beyong their initial area and, either pinch, inversely fold or elongate uniformly (see Appendix Section 2.3). We can map the *polar snoe* because planar markers that are larger or smaller than their initial area are easily distinguished. We could also map the *polar snoie* if it were possible to distinguish folding from unfolding competent veins, or mullioning from unmullioning incompetent sheets. However, we cannot.

If buckles did not unfold as readily as they fold, then veins in or near the *polar snoe* might show boudinaged folds (De Sitter 1958, Passchier 1990b). Boudinaged folds are occasionally reported- but most are attributed to separable rather than progressive deformations. Laboratory experiments (Ramberg 1963, Ghosh 1966) and field observations (Talbot 1970) have shown that competent veins unfold as readily as they fold during progressive bulk strains; folding is completely reversible. Similarly, experiments suggest that, unless they are shortened beyond 70% and become flamed or horned, mullions also re-open on elongation (Sokoutis 1987). Furthermore, our field observations of hundreds of incompetent dykes in the Singö zone failed to distinguish any differences between mullions that were still shortening from those that were elongating but had not yet recovered their initial length. We therefore infer that mullions unmullion as readily as folds unfold.

In effect, because we have never been able to distinguish either unfolding from folding veins, or unmullioning from mullioning dykes, we have not yet been able to directly map the infinitesimal *polar snoie*. Passchier (1990b) suggested overcoming such an impasse by assuming that the *snoie* (or *polar snoie*) lies on the same strain path as the *snoe* (or *polar snoe*). Because our data from the Singö shear zone lie on a straight strain path on a Flinn plot, such a course appears reasonable at first sight. However, replotting our data on the Hsü deformation plot casts doubt on the wisdom of assuming the geometry of the *polar snoie*. Having been so pessimistic about direct mapping of infinitesimal *polar snoies*, the next section suggests that data patterns near the finite *polar snoe* might instead indicate the spin of localities.

1.4. *Rotational bulk strains or spin.* Because most planes rotate during most bulk strains, *polar snoes* generally shrink towards a Z axis that is stationary (in an irrotational bulk strain) or moving (in a rotational bulk strain). During bulk shears that are both progressive and irrotational, poles to material markers all pass through the *polar snoe* in the same direction so that layers previously smaller in area can all later increase. By contrast, *rotational* bulk strains can be thought of in terms of poles to single layers (and their *polar snoe*) shrinking towards a Z axis that is also migrating across an equal-area net (Talbot 1987). The *polar snoe* rotates but the *polar snoie* does not. This means that rotational bulk strains can lead to poles of some veins rotating **out** of the *polar snoe*. Rather than boudinaged folds, we might in this case expect folded boudins near the trailing edge of the *polar snoe* and examples (e.g. Fig. 7f) are not uncommon (e.g. Von Brunn & Talbot 1986, Talbot & Heeroma 1989). The symptoms of rotational bulk strains therefore lie in the finite *polar snoe* rather than in the infinitesimal *polar snoie*.

1.5. *Spin from patterns of data in polar snoes.* The addition of new marker layers during progressive bulk strains can lead to poles of new and undeformed planar layers plotting among poles to folded layers (Talbot 1970, Hutton 1982). Such mixtures of data are expected all the way around *polar snoes* due to irrotational strains but only at the leading edges of *polar snoes* due to rotational bulk strains.

Because folds and mullions are recoverable, mixtures of strain data from inherited planar subfabrics are only likely as a result of rotational bulk strains (spins). All the locality ellipsoids measured in the Singö zone must have spun- but the only symptom of bulk rotational strain recognizable on the scale of the localities are *polar snoes* longer than 90° (Talbot 1987), *polar snoes* with poles to shortened and elongated layers mixed near their leading edges (± poles to folded boudins at their trailing edge), or, as we saw in the Singö zone but excluded from this work, *polar snoes* that are noticeable non-elliptical in shape (pear or mushroom-shaped). Another potential symptom that we saw but excluded is where not all the structural vergence symmetries coincide with the principal planes of strain indicated by the *polar snoe* alone.

2. *Finite macroscopic strains are easier to recognize than infinitesimal strains.*

2.1. *Polar snoes are easier to map than expected.* Flinn (1962, p. 405) did not expect strain ellipsoids to be recoverable using planar fabrics because he expected that small deformations would clear equal-area nets of poles to planar markers (see also Weijermars 1993). However, all the potential complications mentioned earlier arise because material lines rotate faster than the immaterial lines defining the *polar snoe*. This means that even where $\bar{\varepsilon}_s \approx 2.3$ and half the poles to an initially random population have concentrated to within 10° of Z, their *polar snoe* is still likely to be visible because its radius is still only 11° (Talbot 1970, p. 69). In practice, we find that mullions still constrain *polar snoes* up to $\bar{\varepsilon}_s \approx 2.9$ (locality 15). Only at higher strains do all dykes appear to be elongated (as in Fig. 7b).

2.2. *The most common deformation structures in single layers.* If rocks read textbooks we would not be able to map the *polar snoe* as easily and directly as we do. Instead of plotting poles to dykes that have changed in area, we would instead have to map the *snoe* by plotting changes in lengths of lines. This is because the most common structures are not those expected in existing theory.

Single layers in most orientations are expected to both elongate and shorten in different directions at the same time during most progressive bulk strains. As a result, De Sitter (1958), Flinn (1962), Ramsay (1967) and Ramsay & Huber (1983, whose fig. 4.10 is reproduced here as Fig. A1a) expected the most common structure in competent single layers to be 'fold axis normal to boudinage axis'. This is not the case.

We are not aware of any reports of contemporaneous folds and pinches in the same layer. Instead of being confined to two lines (and not illustrated) on Ramsay's diagram (Fig. A1a). Flinn's special cases of 'fold or boudin axes normal to no structure' are in fact the most common structures and expand to fill fields 2a and 2b shown in Fig. A1(b). Talbot's (1970) inference was that pinching might require extension in all directions. However, unpublished experiments at Uppsala demonstrate that plastic layers still pinch and separate to boudins when elongated in bulk simple shear (J. Bergman, personal communication 1989). A more likely rationalization is therefore, that, rather than having two instabilities amplifying together, whichever of the two is dominant entirely swamps the other so that the most common structures in competent single layers are 'folds *or* pinches normal to no structure' (Fields 2a and 2b on Fig. A1b).

By simple analogy to Fig. A1(a), the most common structures in incompetent single layers might be expected to be contemporaneous mullions and inverse folds with axes in different directions. However, we have never noticed mullions and inverse folds in the same dyke. Indeed, we must emphasize that inverse folds are very rare. This is in accord with Smith's (1977) finding that shear instabilities leading to mullions are much weaker than those leading to buckles and that inverse folds are the least likely of all the four potential interference structures. We must also emphasize that we have not seen either the double inverse folds illustrated in Field 1 of Fig. A1(b), or the logically more likely double axis mullions in Field 3.

In summary, single or double axis folds or mullions appear to develop in strain-active single layers that are smaller than their initial area while single or double axis pinches or inverse folds appear in layers that are larger than their initial area.

2.3. *Pinches, inverse folds or 'no structures'?* Two factors control whether perturbations amplify or diminish in strain active interfaces changing in area; the viscosity across them and their orientations in the bulk strain (Talbot 1970, Mandal *et al.* 1992). A third factor controls whether cusp interference across strain-active single layers amplify to folds, mullions, pinches or inverse folds: the layer thickness.

Thick plastic layers elongate as fast as their surroundings by thinning only locally, in pinches (Fletcher 1982). Flinn (1962) expected planar layers (with 'no structures normal to no structures') to be extremely rare because the only planar *snoes* they could parallel result from isochoric biaxial shears. However, in our experience, it is common for

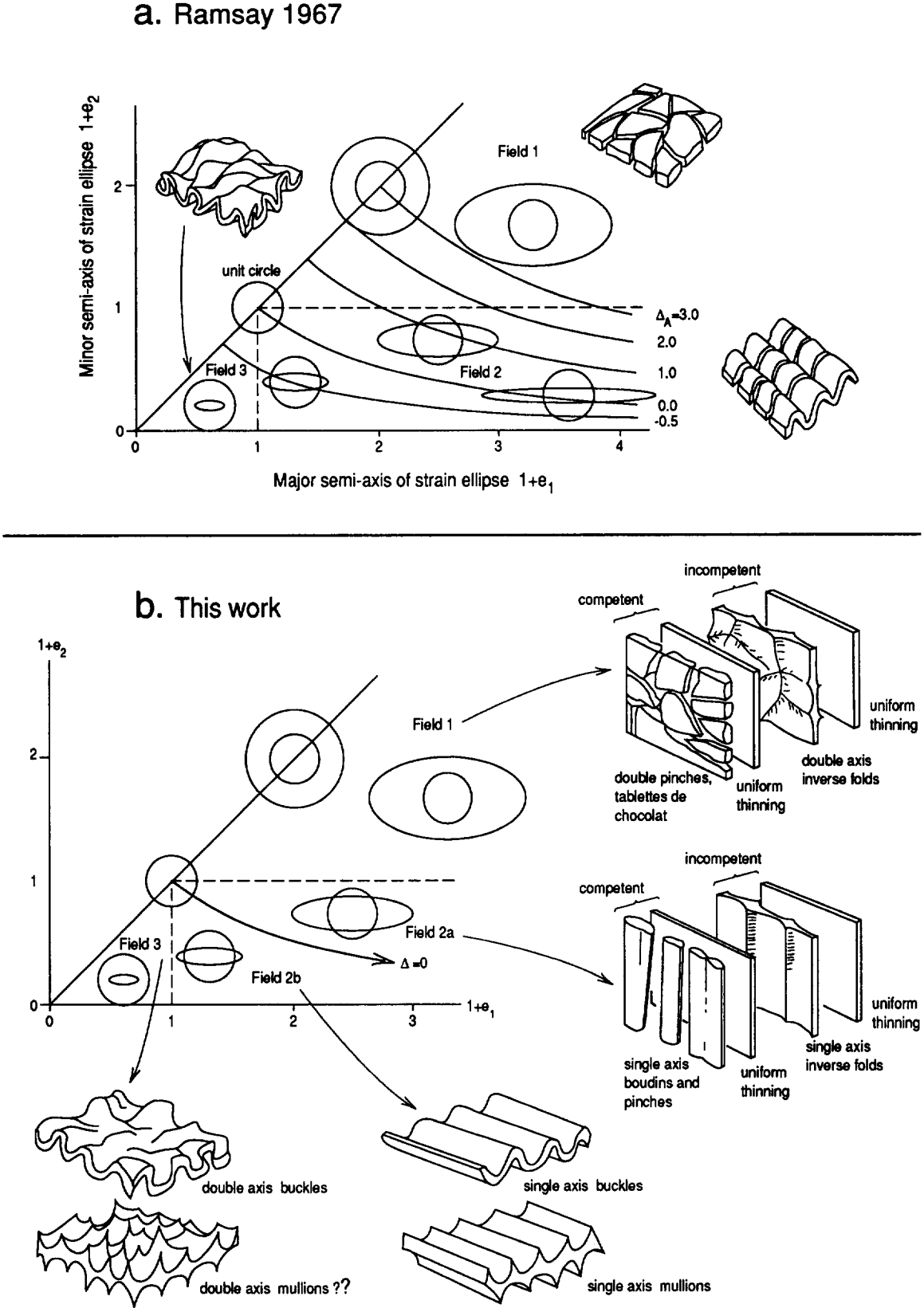

Fig. A1.

single layers to undergo stable elongation so that they thin uniformly to planar layers (Fig. A1b).

Just as poles to thin and uniformly elongated (planar) *competent* veins plot without pattern among poles to thicker pinched or boudinaged veins inside the *polar snoe* (Talbot 1970), so poles to thin and planar *incompetent* dykes are characteristically mixed with poles to even fewer inversely folded dykes. Such a lack of pattern demonstrates that whether perturbations amplify or diminish in a particular population of elongated single layers in the same country rocks depends more upon the layer thickness than their degree of elongation.